Entanglement and decoherence of *N* atoms and a mesoscopic field in a cavity

T. Meunier
Kavli Institute of Nanoscience, Delft University of Technology, P.O. Box 5046, 2600 GA Delft, The Netherlands

A. Le Diffon, C. Ruef, and P. Degiovanni
CNRS-Laboratoire de Physique de l'Ecole Normale Supérieure de Lyon, 46, Allée d'Italie, 69007 Lyon, France

J.-M. Raimond
Laboratoire Kastler Brossel, Département de Physique de l'Ecole Normale Supérieure, 24 rue Lhomond, F-75231 Paris Cedex 05, France

(Received 20 March 2006; published 6 September 2006)

We investigate the behavior of *N* atoms resonantly coupled to a single electromagnetic field mode sustained by a high quality cavity, containing a mesoscopic coherent field. We show with a simple effective Hamiltonian model that the strong coupling between the cavity and the atoms produces an atom-field entangled state, involving $N+1$ nearly coherent components slowly rotating at different paces in the phase plane. The periodic overlap of these components results in a complex collapse and revival pattern for the Rabi oscillation. We study the influence of decoherence due to the finite cavity quality factor. We propose a simple analytical model, based on the Monte Carlo approach to relaxation. We compare its predictions with exact calculations and show that these interesting effects could realistically be observed on a two or three atoms sample in a 15 photon field with circular Rydberg atoms and superconducting cavities.

DOI: 10.1103/PhysRevA.74.033802 PACS number(s): 42.50.Pq, 03.65.Yz, 42.50.Ct, 42.50.Dv

I. INTRODUCTION

Cavity quantum electrodynamics experiments with circular Rydberg atoms and superconducting cavities are well suited for the realization of tests of fundamental quantum processes and of simple quantum information processing functions [1]. They make it possible, in particular, to prepare mesoscopic quantum superpositions, made of coherent field components with different classical attributes (phase and amplitude). They have opened the way to studies of the decoherence dynamics on these states, at the quantum/classical boundary [2]. These early experiments, involving fields containing a few photons only, were based on the dispersive atom-field interaction. The atom, off resonance with the cavity mode, behaved as a state dependent transparent dielectrics modifying transiently the cavity frequency and, hence, the field phase. An atom in a superposition of levels produces then a quantum superposition of phase shifts, a situation reminiscent of the famous Schrödinger cat situation.

Much faster phase shifts can be realized through the resonant atom-cavity interaction. The complex Rabi oscillation phenomenon in a mesoscopic field results in an atom-field entanglement induced by photon graininess. The initially coherent cavity field is rapidly cast in a superposition of two components with different phases. This phase splitting is a mesoscopic effect that disappears in the classical limit of a very large field, which is then left unaffected by the atoms. This resonant phase splitting effect has been evidenced for fields containing up to a few tens of photons [3]. Its coherence has been checked using an echo technique borrowed from NMR [4], following a proposal by Morigi *et al.* [5]. The resonant atom-field interaction thus opens the way to decoherence studies with large photon numbers. These experiments focused on a simple situation with a single atom coupled to the cavity mode. Recent experimental advances [6] allow us to envision experiments with samples containing a well known number $N>1$ of atoms. They would merge the concepts of cavity QED with the atomic ensemble manipulations recently put forth for quantum information processing. In this context, it is particularly interesting to study the resonant interaction of such a multiatom sample with a mesoscopic field.

In this paper, we study the resonant interaction of an atomic ensemble of *N* atoms with a cavity initially prepared in a mesoscopic coherent state. Using an appropriate mesoscopic approximation, we show that the strong atom/field interaction leads to an entangled atom-field state involving $N+1$ nearly coherent field components with different classical phases, generalizing the results obtained for one atom [7]. These coherent components are correlated with dipole atomic states, superpositions of the upper and lower states with equal weights. Thus, in the mesoscopic limit, the cavity field acts as a which-path detector for the atomic states interference. The periodic partial disentanglement of the atom-field system due to the transient overlap of field components is then closely linked to the complex pattern of quantum Rabi oscillation collapses and revivals observed in this regime. As in the single atom case, early quantum revivals can be induced by an echo sequence, realizing a time reversal of the atom-field evolution [5]. The experimental observation of these effects would shed light on the deep links between entanglement and complementarity.

This complex phase splitting was already predicted by Knight and Shore [8]. In the present paper, the introduction of an effective Hamiltonian valid in the mesoscopic domain enables us to capture the main results within a simple analytical model. This approach, originally pioneered by Klimov and Chumakov [9], is also instrumental in the discussion of dissipation in the system.

Dissipation in the cavity turns the entangled atoms-field state into a statistical mixture, destroying Rabi oscillation revivals. In order to assess the experimental accessibility of these mesoscopic quantum effects, we have analyzed quantitatively the influence of cavity dissipation on the evolution of the atom-cavity entangled state. Using the physical insight provided by the stochastic wave function approach [10] to the dissipative dynamics of the atoms + cavity system, an analytic formula for the decoherence of the mesoscopic atoms + cavity state is derived. It generalizes to the case of $N>1$ atoms the results previously obtained by Gea-Banacloche [11] in the $N=1$ case. We provide a functional expression for the decoherence coefficients of the entangled atoms + cavity state which is valid even in the presence of an echo sequence used to induce an early revival of the quantum Rabi oscillation. The functional form of these decoherence coefficients reflects the cumulative construction of the imprint left by the strongly coupled atoms + cavity system in the cavity environment. These physically illuminating expressions can be straightforwardly generalized to compute decoherence properties during a more complex protocol, such as the injection of another atomic ensemble in the cavity shortly after the first one in order to probe the cavity field.

The organization of this paper is as follows. In Sec. II, the model for the resonantly coupled atoms + cavity system is presented and its dynamics is studied in the absence of dissipation using a mesoscopic approximation in the spirit of Gea-Banacloche [7]. In Sec. III, dissipation of the cavity is introduced and studied analytically using the stochastic wave function approach. Section IV presents numerical results obtained from quantum Monte Carlo simulations. These results are used to discuss experimentally accessible windows for the observation of a mesoscopic entanglement between two or three atoms in a microwave high quality cavity in the near future. We also comment on the possibility of observing such mesoscopic effects within the context of circuit-QED experiments performed with nanofabricated superconducting circuits [12]. The next generation of these experiments will involve several qubits coupled to a cavity. Therefore, it is very natural to address the question of entanglement between several qubits and the resonator for circuit-QED devices.

II. HAMILTONIAN EFFECTIVE DYNAMICS IN THE MESOSCOPIC REGIME

A. The Tavis-Cummings model

In this paper, the resonant interaction between N two-level atoms and an electromagnetic mode in a cavity is considered. The cavity mode is modeled by a quantum harmonic oscillator which, in Sec. III, will be weakly coupled to an harmonic bath representing its environment.

Assuming that all atoms are symmetrically coupled to the mode, the atom-field system is conveniently described by the Tavis-Cummings model [13], a spin $J=N/2$ generalization of the Jaynes-Cummings model [14]. The interaction between the atoms and the electromagnetic mode is given by

$$H=\frac{\hbar g}{2}\sum_{i=1}^{N}(S_i^+a+S_i^-a^\dagger), \tag{1}$$

where $S_i^\pm$ denote the raising and lowering operators for the ith atom. The energy scale associated with the interaction of one atom with the mode is $\hbar g$. Because of the symmetric coupling, the evolution is restricted to the symmetric subspace, invariant under atomic permutations, provided the initial state is also symmetric, a condition that we assume fulfilled from now on. The atomic degree of freedom is the spin $J=N/2$ representation for the collective su(2) generators

$$J^z=\sum_{i=1}^{N}S_i^z,\quad J^\pm=\sum_{i=1}^{N}S_i^\pm. \tag{2}$$

The interaction Hamiltonian can then be rewritten in terms of these operators leading to the Tavis-Cummings (TC) model

$$H_{\mathrm{TC}}=\frac{\hbar g}{2}(J^+a+J^-a^\dagger). \tag{3}$$

Within this framework, the atomic ensemble behaves as a collective quantum object, a spin $J=N/2$ interacting with a quantum harmonic oscillator. A convenient basis in the atom + cavity Hilbert space is made up of tensor products of the atomic Dicke states $|J,m\rangle$, common eigenstates of J^2 and J^z, and the Fock states $|n\rangle$ for the harmonic oscillator. Note that the Hilbert space for this coupled system contains stable subspaces under time evolution which organize as follows: first, an infinity of $(2J+1)$-dimensional subspaces $\mathcal{H}_n$ $(n\geq 0)$ generated by the states $|J,J-l\rangle\otimes|n+l\rangle$, where l ranges from 0 to $2J$. Then, a finite number of lower dimension subspaces indexed by $-J\leq m<J-1$ generated by $|J,m-l\rangle\otimes|l\rangle$, where $0\leq l\leq J-m$.

In this paper, we focus on the mesoscopic regime in which the exchange of quanta between the collective state of the N atoms and the cavity mode does not significantly alter the latter. Since the collective atomic spin can transfer at most N photons to the electromagnetic mode, this implies $\bar{n}\gg N$, where $\bar{n}$ is the mean photon number in the cavity.

B. Mesoscopic entanglement involving one atom in a cavity

1. Mesoscopic approximation for the atom + cavity evolution

The quantum dynamics of a single atom interacting with a coherent state in a cavity has been investigated by Gea-Banacloche [7] and independently by Buzek and Knight [15]. The analysis by Gea-Banacloche is based on the exact diagonalization of the Jaynes-Cummings Hamiltonian. It provides an approximate solution for the Schrödinger equation with the initial condition $|\psi_{\mathrm{at}}\rangle\otimes|\alpha\rangle$ where $|\psi_{\mathrm{at}}\rangle$ denotes the initial state of the two-level atom and $|\alpha\rangle$ is a coherent state of the cavity field containing a mesoscopic number $\bar{n}=|\alpha|^2$ of photons $(\alpha=\sqrt{\bar{n}})$.

The atom + field interaction is expected to create an entangled state. As noticed by Knight and Shore, using an argument based on the Schmidt theorem [8], a two-level atom cannot get entangled with more than two orthonormal states of the field. The Gea-Banacloche approximate solution precisely expresses the atom + field state $|\Psi(t)\rangle$ at time t as a two-component entangled state. As discussed by Gea-Banacloche [7], this approximation is accurate for $t\ll\bar{n}/g$ which, for $\bar{n}\gg 1$, is large compared to the vacuum Rabi period $2\pi/g$. It leads to

$$|\Psi(t)\rangle = Ae^{-igt\sqrt{\bar{n}}/2}|D_+(t)\rangle \otimes |\psi_+(t)\rangle + Be^{igt\sqrt{\bar{n}}/2}|D_-(t)\rangle \otimes |\psi_-(t)\rangle, \quad (4)$$

where A and B characterize the initial atomic state ($|e\rangle$ in recent experiments [4]). The atomic dipole states $|D_\pm(t)\rangle$ are given by

$$|D_\pm(t)\rangle = \frac{1}{\sqrt{2}}(\pm e^{\mp igt/4\sqrt{\bar{n}}}|+\rangle + |-\rangle) \quad (5)$$

and the field states $|\psi_\pm(t)\rangle$ are

$$|\psi_\pm(t)\rangle = e^{\pm igt\sqrt{\bar{n}}/2}e^{-\bar{n}/2}\sum_{k=0}^{\infty}\frac{\alpha^k}{\sqrt{k!}}e^{\mp igt\sqrt{k}/2}|k\rangle. \quad (6)$$

In the following, we will use the short hand denomination "Gea-Banacloche states" for these cavity states and their generalization to $N>1$.

2. Discussion

Gea-Banacloche has also shown that, for times short compared to $g^{-1}\sqrt{\bar{n}}$, the state $|\psi_\pm(t)\rangle$ can be approximated by a coherent state of parameter $\alpha_\pm(t)=e^{\mp igt/4\sqrt{\bar{n}}}\alpha$. This result is obtained by expanding $\sqrt{k}$ at first order in $k-\bar{n}$ around $\sqrt{\bar{n}}$ leading to

$$|\psi_\pm(t)\rangle \simeq e^{\pm igt\sqrt{\bar{n}}/4}|\alpha e^{\mp igt/4\sqrt{\bar{n}}}\rangle \quad (7)$$

in the limit $t \ll \sqrt{\bar{n}}/g$. Thus, the states $|\psi_\pm(t)\rangle$ mainly evolve at slow frequencies $\pm g/4\sqrt{\bar{n}}$. We refer to Eq. (7) as the "coherent state approximation" for Gea-Banacloche states and, if inserted in Eq. (4), as the coherent state approximation for the atom + cavity system. As discussed in details in Ref. [7], this approximation breaks down for $t \gtrsim \sqrt{\bar{n}}/g$ because the states $|\psi_\pm(t)\rangle$ undergo a slow phase spreading due to higher order terms in their expansion. They can no longer be considered as coherent. However, even if it breaks down before the mesoscopic approximation, the coherent state approximation provides a nice intuitive and pictorial support for visualizing the system's evolution.

With this image in mind, it is useful to draw on the same diagram the motion of the average atomic polarization $\vec{d}_\pm(t)=\langle D_\pm(t)|\vec{\sigma}|D_\pm(t)\rangle$ in the equatorial plane of the Bloch sphere and the motion of $\alpha_\pm^*(t)$ in the Fresnel plane. The result is depicted on Fig. 1 for $\varphi=0$: the corresponding vectors rotate at angular velocity $\pm g/4\sqrt{\bar{n}}$, small compared to the classical Rabi frequency $g\sqrt{\bar{n}}$.

In the limit $\bar{n}\to\infty$ and $gt \ll 1$, both states $|\psi_\pm(t)\rangle$ are close to $|\alpha\rangle$ for $t \ll g^{-1}$, meaning that the cavity mode is barely affected by the atoms. In this regime, the cavity state factors out and the atomic polarizations $|D_\pm(t)\rangle$ coincide with the atomic spin-1/2 eigenstates along the x direction. These atomic states interfere resulting in the classical Rabi oscillation phenomenon. Remember that the period of classical Rabi oscillations is of the order $g^{-1}/\sqrt{\bar{n}}$. Therefore, in the classical limit $\bar{n}\to+\infty$, more and more oscillations take place before the motion of Gea-Banacloche states in the phase plane has any measurable consequence.

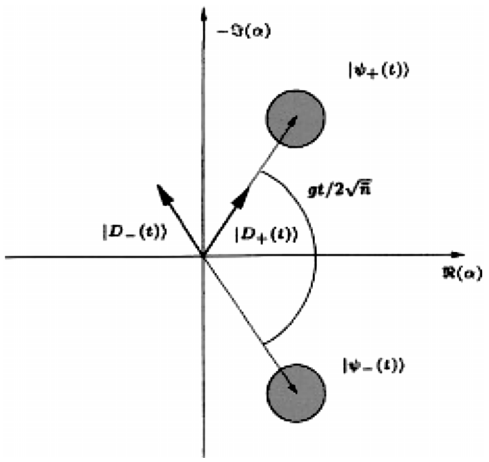

FIG. 1. Schematic evolution of the entangled state for one atom and a mesoscopic coherent state in a cavity for real positive α. The atomic dipole states are represented as arrows. The field coherent states are represented as an uncertainty disk at the tip of the classical amplitude. Each component $|D_\pm(t)\rangle\otimes|\psi_\pm(t)\rangle$ of the superposition involves an atomic polarization and a field state slowly rotating in the phase plane at velocities $\pm g/4\sqrt{\bar{n}}$.

In the mesoscopic regime (fixed $\bar{n}\gg 1$), the state of the cavity is altered by the atom. Interferences between atomic polarizations $|D_\pm(t)\rangle$ can only be observed when $|\psi_+(t)\rangle$ and $|\psi_-(t)\rangle$ overlap. As explained above, at very short times, these states are still close to the initial coherent state $|\alpha\rangle$. When the phase separation between $|\psi_+(t)\rangle$ and $|\psi_-(t)\rangle$ due to their slow rotation in phase space is larger than the quantum phase fluctuations in these coherent components ($gt/2\sqrt{\bar{n}} \sim 1/\sqrt{\bar{n}}$), the cavity field behaves as a *bona fide* "path detector" for the atomic polarizations and Rabi oscillations disappear. The Rabi oscillation collapses after a time of the order of the vacuum Rabi oscillation, after $\sqrt{\bar{n}}$ classical oscillations.

The Rabi oscillation signal reappears when $|\psi_+(t)\rangle$ and $|\psi_-(t)\rangle$ overlap again. This happens for $gt/2\sqrt{\bar{n}}\simeq 2\pi$. During this overlap, the disentanglement of the atom + cavity state erases the information stored in the cavity about the path followed by the atomic degrees of freedom. This "quantum eraser situation" leads to a revival of Rabi oscillations. Rabi oscillation revivals in the mesoscopic regime are thus a direct application of the complementarity concept [16]. Figure 2 shows, as a function of the dimensionless time $\phi = gt/2\sqrt{\bar{n}}$, the first spontaneous revival of the Rabi oscillation signal obtained by numerical integration of the Schrödinger equation for one atom initially in the excited state and coherent states of 14 and 40 photons in average.

3. The echo protocol

The echo protocol proposed by Morigi [5] aims at testing the coherence of the atom + cavity state by a time reversal operation. A percussional echo pulse is applied to the atom at time t_π. It corresponds to the unitary operator $U_\pi=i\sigma^z$. The evolution for the atom + cavity system up to time $t \geq t_\pi$ is then given by

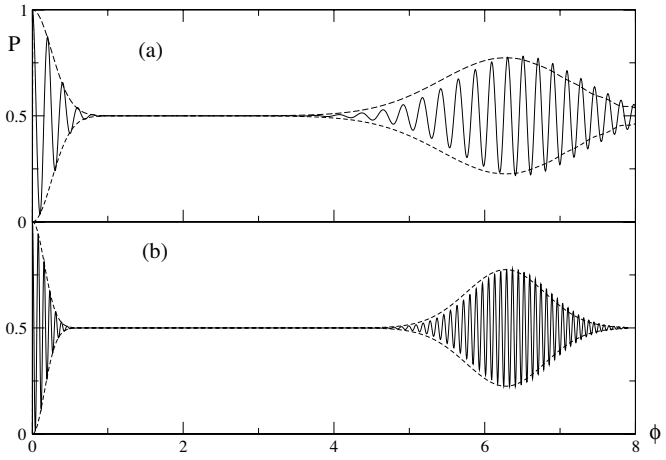

FIG. 2. Spontaneous revivals of the Rabi oscillation signal for one atom with initial condition $(|e\rangle=|m=1/2\rangle)\otimes|\alpha\rangle$ and a coherent state with mean photon number (a) $\bar{n}=15$ and (b) $\bar{n}=40$. The solid line shows the probability $P(\phi)$ for finding the atom in $|e\rangle$, as a function of the dimensionless time $\phi=gt/2\sqrt{\bar{n}}$, computed using numerical integration. The dashed curves show the upper and lower envelopes predicted by our mesoscopic approximation.

$$U(t) = e^{-i(t-t_\pi)H/\hbar} U_\pi e^{-it_\pi H/\hbar}, \tag{8}$$

where H is the Jaynes-Cummings Hamiltonian. Using $U_\pi^2 = 1$ and $U_\pi H U_\pi = -H$, we get

$$U(t) = U_\pi e^{-i(t_\pi - t)H/\hbar} e^{-it_\pi H/\hbar}. \tag{9}$$

Therefore, right after the echo pulse, the Gea-Banacloche states reverse their evolution and recombine at $2t_\pi$ leading to an induced Rabi oscillation revival. This induced revival may occur at much shorter time than the "spontaneous" revival, making its experimental observation much easier, as shown recently [4]. Moreover, in the absence of decoherence, the induced revival should occur with unit contrast. The influence of decoherence could thus be, in principle, directly assessed from the measurement of the induced revival contrast.

4. Towards atomic ensembles

In this paper, we are interested in studying the resonant interaction of an atomic ensemble containing $N>1$ atoms with a mesoscopic field in a cavity. Invoking again Schmidt theorem [8], we expect this resonant interaction to create an entangled state with $2J+1=N+1$ orthonormal components. As in the one-atom case, partial disentanglement of this state will lead to spontaneous revivals of Rabi oscillations.

An analytic diagonalization of the Tavis-Cummings Hamiltonian can be obtained for $N=1,2,3$ but not for greater values of N. Moreover, as will be clear from forthcoming sections, the analytical diagonalization for these values of N does not enlighten the dynamics of the system. In particular, for $N>1$, the explicit expressions of exact eigenstates in the resonant Tavis-Cummings Hamiltonian depend on N. This direct approach thus cannot be used as a convenient starting point for an approximate solution of the Schrödinger equation for $N>1$.

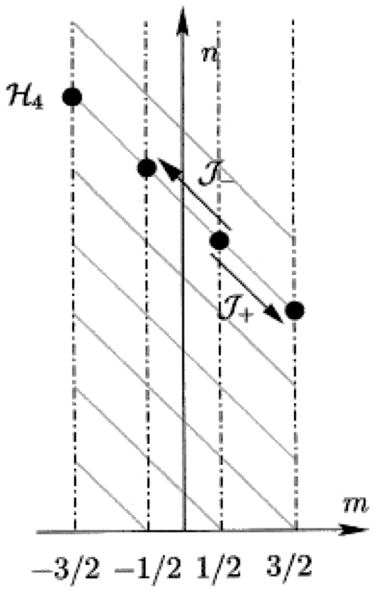

FIG. 3. Schematic view of the Hilbert space for $N=3$ atoms. The oblique gray lines represent the stable subspaces. The action of $\mathcal{J}_\pm$ on $\mathcal{H}_3$ is depicted.

Our approach, developed in the next section, relies on an effective Hamiltonian which, in the mesoscopic domain, provides an excellent approximation to the Tavis-Cummings Hamiltonian. It provides a unified vision of the dynamics for all values of N and as such, it is a good starting point for analyzing the dynamics in the mesoscopic domain. As we shall see, in this framework, the dynamics of the resonant Tavis-Cummings model can then be described in the spirit of the Gea-Banacloche approach.

C. Effective dynamics in the mesoscopic domain

1. Effective Hamiltonian

First of all, let us remark that any initial state of the form $|J,m_0\rangle\otimes|\alpha\rangle$ in the mesoscopic domain mainly spreads over $(2J+1)$-dimensional stable subspaces $\mathcal{H}_n$ for values of n around $\bar{n}$. The core of our approach is to replace the Tavis-Cummings Hamiltonian (3) acting on subspaces $\mathcal{H}_n$ by an effective Hamiltonian in which the n dependence factors out. It appears that the main n dependence of Eq. (3) scales as $\sqrt{n}$ for large values of n. As in the $N=1$ case, this nonlinearity leads to the collapse of the Rabi oscillations and the discrete character of the spectrum leads to spontaneous revivals.

In order to describe our ansatz for the effective Hamiltonian, it is convenient to remark that each subspace $\mathcal{H}_n$ can be turned into a spin-J representation of su(2). Let us introduce new operators $\mathcal{J}^\pm$ and $\mathcal{J}^z$. With the notation $|Z_m^{(n)}\rangle = |J,m\rangle\otimes|n+J-m\rangle$, these new operators simply act on these states in the same way as standard su(2) generators act on the $|J,m\rangle$ states $\mathcal{J}^\pm|Z_m^{(n)}\rangle = \sqrt{J(J+1)-m(m\pm1)}\,|Z_{m\pm1}^{(n)}\rangle$ (see Fig. 3). The operators aJ^+ and $a^\dagger J^-$ then act on the states $|Z_m^{(n)}\rangle$ as

$$aJ^+|Z_m^{(n)}\rangle = \sqrt{n+J-m}\,\mathcal{J}^+|Z_m^{(n)}\rangle, \tag{10}$$

$$a^{\dagger}J^{-}|Z_m^{(n)}\rangle = \sqrt{n+J-m+1}\,\mathcal{J}^{-}|Z_m^{(n)}\rangle. \tag{11}$$

We then note that computing the evolution of a state $|J,m\rangle \otimes |\alpha\rangle$ in the mesoscopic regime requires considering values of n close to $\bar{n} \gg N$. The variation of $\sqrt{n+k}$ for $0 \leq k \leq N+1$ is small for $n \gg N$ (of the order of $N/\sqrt{\bar{n}}$). We thus drop the m dependence of $\sqrt{n+J-m}$ and $\sqrt{n+J-m+1}$ by replacing them by $\sqrt{n+c}$, where $0 \leq c \leq N+1$ is a constant to be discussed in the next paragraph. This leads to an effective Hamiltonian of the form

$$H_{\text{eff}}^{(n)} = \frac{\hbar g}{2}\sqrt{n+c}(\mathcal{J}^{+}+\mathcal{J}^{-}) = \hbar\, g\sqrt{n+c}\,\mathcal{J}^{x}. \tag{12}$$

This Hamiltonian, already derived by Klimov and Chumakov [9] and used to study the squeezing of light by an atomic ensemble [17], shares some features with the expected classical dynamics, driven by an effective field along x. Here, however, photon emission and absorption are taken into account through the fact that $\mathcal{J}^{\pm}$ changes the photon number (see Fig. 3). At fixed n, the eigenvalues of this effective Hamiltonian are equally spaced, as predicted by [13] for the Tavis-Cummings Hamiltonian in the large n limit. All the n dependence of this effective Hamiltonian is contained in the $\sqrt{n+c}$ factor.

Of course, there is an ambiguity in the choice of $0 \leq c \leq N+1$ but we shall see that (i) for $N=1$ choosing $c=1$ reproduces the results of Sec. II B and (ii) for $N>1$, changing c only affects the rapidly oscillating part of the Rabi oscillation signal. It does not change its envelope which is precisely the information we hope to extract from the effective Hamiltonian.

2. The mesoscopic approximation

Using this effective Hamiltonian, it is possible to study the evolution of a state $|\Psi_m^X\rangle = |J,m\rangle_x \otimes |\alpha\rangle$, where $J^x|J,m\rangle_x = m|J,m\rangle_x$. An approximate solution for the Schrödinger equation shows that this state remains factorized (see Appendix A for details):

$$|\Psi_m^X(t)\rangle = e^{-imgt|\alpha|}|D_m(t)\rangle \otimes |\psi_m(t)\rangle, \tag{13}$$

where the state of the electromagnetic mode is of the form

$$|\psi_m(t)\rangle = e^{imgt\sqrt{\bar{n}}}e^{-\bar{n}/2}\sum_{k=0}^{\infty}\frac{\alpha^k}{\sqrt{k!}}e^{-imgt\sqrt{k}}|k\rangle, \tag{14}$$

which we call, as above, a Gea-Banacloche state [7]. The atomic polarizations generalize the ones found by Gea-Banacloche in the spin 1/2 case

$$|D_m(t)\rangle = \sum_{m'=-J}^{J} e^{-igmt(c-J+m')/2\sqrt{\bar{n}}}(R^{-1})_{m,m'}|J,m'\rangle, \tag{15}$$

where R denotes the rotation matrix $R_{m,m'} = \langle J,m'|e^{i\pi J^y/2}|J,m\rangle$. Note the presence of the classical Rabi frequencies $mg|\alpha|$ corresponding to the quantum beat between spin eigenstates along the x direction of the effective classical field. The average angular momentum $\vec{d_m}(t) = \langle D_m(t)|\vec{J}|D_m(t)\rangle$ slowly rotates in the equatorial plane of the Bloch sphere at angular velocity $gm/2\sqrt{\bar{n}}$. The parameter c appears in these atomic polarizations only and, for $N=1$, the Gea-Banacloche results are exactly recovered for $c=1$.

Starting from state $|\Psi(0)\rangle = |J,m\rangle \otimes |\alpha\rangle$, an entangled state with $N+1$ components is obtained:

$$|\Psi(t)\rangle = \sum_{m=-J}^{J} R_{m_0,m}e^{-imgt|\alpha|}|D_m(t)\rangle \otimes |\psi_m(t)\rangle. \tag{16}$$

As in the one-atom case, the entangled state (16) can be viewed as the result of the ideal measurement of the spin by the mesoscopic field in the cavity.

3. The coherent state approximation

As in the single-atom case, the state $|\psi_m(t)\rangle$ can be approximated by a coherent state of complex amplitude $\alpha_m(t) = e^{-imgt/2\sqrt{\bar{n}}}\alpha$. This approximation holds in the limit $t \ll (g|m|)^{-1}\sqrt{\bar{n}}$. At longer times, typically $\sqrt{\bar{n}}/g|m|$, the field state gets deformed as the $|\psi_{\pm}\rangle$ states in the $N=1$ case.

With this image in mind, it is useful to draw on the same diagram the motion of the average atomic polarization $\vec{d_m}(t)$ in the equatorial plane of the Bloch sphere and the motion of $\alpha_m(t)$ in the Fresnel plane, generalizing the phase space representation used above. The main difference with the $N=1$ case is the appearance of $N+1$ frequencies and field states instead of two. Here also, the phase of the coherent state plays the role of a pointer measuring the angular momentum of the collective spin along the x direction in the $\bar{n} \gg 1$ limit. Larger angular momenta lead to larger angular velocities. As we shall see now, this complex atoms + cavity entangled state leads to a rich pattern of spontaneous revivals of Rabi oscillations.

D. Partial revivals of Rabi oscillations

1. General picture

Rabi oscillations of the atomic populations provide a nice way to probe the degree of entanglement of the atom + cavity state. In the classical limit ($\bar{n} \to \infty$), the electromagnetic field state factors out and quantum interferences between the various atomic polarizations $|D_m(t)\rangle$ can be observed. They are the Rabi oscillations for the quantum spin J in a transverse classical field.

In the mesoscopic limit, the electromagnetic mode is altered by the atom. Interferences between atomic polarizations $|D_m(t)\rangle$ can only be observed when the corresponding field states $|\psi_m(t)\rangle$ overlap. At very short times, the various components $|\psi_m(t)\rangle$ are still close to the initial coherent state $|\alpha\rangle$ and Rabi oscillations show up. When the various Gea-Banacloche states split apart, the electromagnetic field becomes a good "path detector" for the atomic polarizations and the Rabi oscillations collapse. This is again a complementarity effect, the field storing which-path information about the interfering atomic states. Rabi oscillations reappear when this which-path information is, at least partially, erased, i.e., when some of the Gea-Banacloche states overlap again. In the $N>1$ case, the atoms + cavity state is a super-

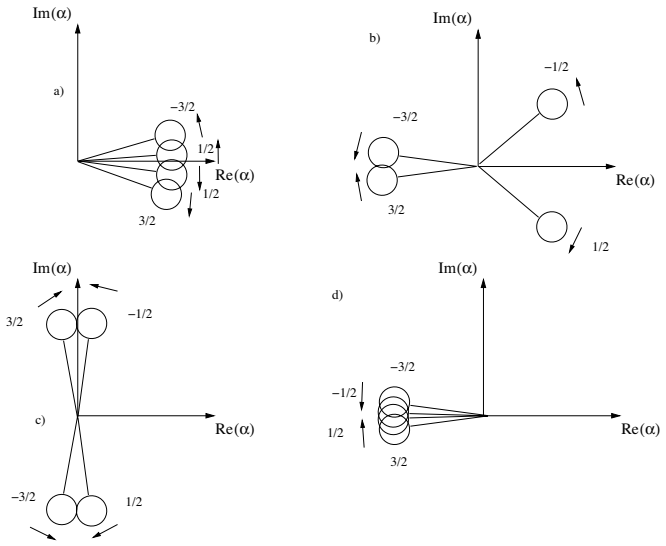

FIG. 4. Position of the Gea-Banacloche states at the times of first occurrence of spontaneous Rabi oscillation revivals for $N=3$ ($J=3/2$). (a) Collapse of the Rabi oscillations when the various components split apart. (b) First spontaneous revival for $\phi=2\pi/3$. (c) Second spontaneous revival for $\phi=\pi$. (d) Complete spontaneous revival involving all atomic polarizations for $\phi=2\pi$.

position of $N+1$ factorized components rotating at different velocities and a rich spontaneous revival pattern is expected.

The angular velocity of the Gea-Banacloche states $|\psi_m(t)\rangle$ in the Fresnel plane is here $-gm/2\sqrt{\bar{n}}$, suggesting to associate with each Rabi oscillation revival a nonempty subset $\mathcal{E}$ of $\{1,\ldots,2J\}$ which is the list of absolute values of differences of the indices m of those Gea-Banacloche states that overlap during the revival under consideration. Given such a subset $\mathcal{E}$, the revival is built from contributions of pairs of states $|\psi_{m_+}(t)\rangle$ and $|\psi_{m_-}(t)\rangle$ such that $|m_+-m_-|\in\mathcal{E}$. Note that, when a pair $|\psi_{m_+}(t)\rangle$ and $|\psi_{m_-}(t)\rangle$ overlaps, all pairs that have a positive or negative integer multiple value of m_--m_+ also overlap. Therefore if q belongs to such a subset, its multiples also do. This is the only constraint on the subsets $\mathcal{E}$. The Rabi oscillation revivals are therefore classified by the greatest common divisor $\gcd(\mathcal{E})$ of the elements of $\mathcal{E}$. The first time of occurrence of the spontaneous revival associated with $\mathcal{E}$ is t such that $gt/2\sqrt{\bar{n}}=2\pi/\gcd(\mathcal{E})$. Replicas of this revival will occur at integer multiples of this fundamental time. Note that there are $N+1-\gcd(\mathcal{E})$ pairs of Gea-Banacloche states that verify $|m_+-m_-|=q$. Remember that $\phi=gt/2\sqrt{\bar{n}}$ is the dimensionless time which characterizes the slow motion of Gea-Banacloche states. In general, the contrast of replicas will be reduced because of the spreading of the Gea-Banacloche state (especially if they occur after $gt/2\sqrt{\bar{n}}\geq 2\pi$). For all values of N, the set $\{1,\ldots,N\}$ corresponds to a complete revival involving the recombination of all Gea-Banacloche states at $\phi=2\pi$.

As an example, let us consider the case of three atoms. The corresponding Rabi revival patterns are depicted on Fig. 4. The first revival is obtained when $m=\pm 3/2$ states overlap for $\phi=2\pi/3$ (associated subset $\mathcal{E}=\{3\}$). It is partial (contrast is lower than one) since only two atomic polarizations take part in it. The next revival appears for $\phi=\pi$ when $m=3/2$ and $-1/2$ and $m=-3/2$ and $1/2$ overlap separately ($\mathcal{E}=\{2\}$). At $\phi=4\pi/3$, $m=3/2$ and $m=-3/2$ recombine again leading to a partial revival which is a replica of the first one ($\mathcal{E}=\{3\}$). Finally the complete revival involving quantum interferences between all four atomic polarizations takes place at $\phi=2\pi$ ($\mathcal{E}=\{1,2,3\}$). Note that the first example of a nontrivial revival involving several slow frequencies before the complete revival occurs for $N=4$ at $\phi=\pi$ ($\mathcal{E}=\{2,4\}$).

2. Rabi oscillation envelopes

Preparing $J+m_0$ atoms in the excited state, the probability of detecting $J+m$ ones in the excited state and $J-m$ in the ground state is given by ($q=m_+-m_-$):

$$P_m(t)=\sum_{m_+,m_-} e^{-igqt\sqrt{\bar{n}}/2}\mathcal{P}^{(m_0,m)}_{m_+,m_-}(t)\mathcal{R}_{m_+,m_-}(t), \tag{17}$$

where $m_\pm$ runs from $-J$ to J and

$$\mathcal{P}^{(m_0,m)}_{m_+,m_-}(t)=R_{m_0,m_+}R^*_{m_0,m_-}\langle J,m|D_{m_+}(t)\rangle\langle D_{m_-}(t)|J,m\rangle \tag{18}$$

contains the matrix elements of atomic polarizations. The scalar products $\langle J,m|D_{m_\pm}(t)\rangle$ can also be expressed in terms of the rotation matrices (see Appendix B for explicit expressions):

$$\langle J,m|D_{m_\pm}(t)\rangle=(R^{-1})_{m_\pm,m}e^{-ig(c-J+m)m_\pm t/2\sqrt{\bar{n}}}. \tag{19}$$

Within our effective Hamiltonian approximation, the time dependence of the atomic polarization factor $\mathcal{P}^{(m_0,m)}_{m_-,m_+}$ is a phase. Modulation factors for the revivals come from the overlaps of cavity mode states

$$\mathcal{R}_{m_+,m_-}(t)=\langle\psi_{m_-}(t)|\psi_{m_+}(t)\rangle. \tag{20}$$

This expression only depends on $q=m_+-m_-$. Finally, the Rabi oscillation signal is

$$P_m(t)=\sum_{q=-2J}^{2J}\mathcal{R}_q(t)\mathcal{A}^{(m_0,m)}_q e^{-i(gqtc/2\sqrt{\bar{n}})}e^{-igqt\sqrt{\bar{n}}}, \tag{21}$$

where

$$\mathcal{A}^{(m_0,m)}_q=\sum_{m_--m_+=q}R_{m_0,m_+}R^*_{m_0,m_-}R^{-1}_{m,m_+}(R^{-1}_{m,m_-})^*.$$

This expression separates the rapid frequencies $gq\sqrt{\bar{n}}$ from the mesoscopic slow frequencies $gq/2\sqrt{\bar{n}}$. The Rabi signal then consists into a rapidly oscillating signal slowly modulated in amplitude and phase. Expression (21) can be used to find an approximate analytic expression for the upper and lower envelopes of the signal. Let us illustrate this point on the signal obtained for $m_0=m=J$ (denoting $\mathcal{A}^{(J,J)}_q=\mathcal{A}_q$) which is plotted in the forthcoming figures.

Outside the spontaneous revivals, the contribution of the $q\neq 0$ terms in Eq. (21) vanishes. The base line of the Rabi oscillation signal is thus $\mathcal{A}_0$. Obtaining the envelopes is trivial for $N=1$ since there is exactly one value of q involved: $q_r=1$. The slowly varying phase $e^{-igqtc/2\sqrt{\bar{n}}}$ simply shifts the rapid oscillation without changing its envelope.

This analysis is also correct for $N>1$ in the case of a revival involving exactly one frequency corresponding to $q_r \in \{1,\ldots,N\}$ ($q_r=1$ for $N=1$). For these revivals only, the upper and lower envelopes P_+ and P_- take the form

$$P_{\pm}(t) = \mathcal{A}_0 \pm |\mathcal{R}_{q_r}(t)\mathcal{A}_{q_r}|. \tag{22}$$

Thus, simple revivals are symmetric with respect to the flat signal $\mathcal{A}_0$ and involve only one rapid frequency $gq_r\sqrt{\bar{n}}$.

The analysis turns out to be more involved when several frequencies are involved. A first example of this situation is the initial collapse of Rabi oscillation ($t \lesssim 2\pi/g$) for $N>1$. Nevertheless, the envelopes can be obtained using the exact expression for classical Rabi oscillation in a field of amplitude $\sqrt{\bar{n}}$: in this limit, the probability for detecting all atoms in the excited state is given by $P_c(t)=\cos^{2N}(gt\sqrt{\bar{n}}/2)$. Its maxima occur at times $2\pi k/g\sqrt{\bar{n}}$ for integer values of k and its minima occur for half integer values of k. Substituting these values in Eq. (21) for large values of $\bar{n}$ provides the values of the rapidly oscillating term to be used to fit the maxima (upper envelope) and the minima (lower envelope). This leads to

$$P_+(t) = \mathcal{A}_0 + \sum_{q\neq 0} |\mathcal{R}_q(t)\mathcal{A}_q|, \tag{23}$$

$$P_-(t) = \mathcal{A}_0 + \sum_{q\neq 0} (-1)^q |\mathcal{R}_q(t)\mathcal{A}_q|. \tag{24}$$

Note that for $N>1$, the envelope is not symmetric with respect to the flat signal $\mathcal{A}_0$.

Let us now turn to the complete revival which takes places around $t_R=4\pi\sqrt{\bar{n}}/g$. Near this revival, the Rabi oscillation signal takes the form ($t=t_R+\tau$):

$$P(t) = \mathcal{A}_0 + \sum_{q\neq 0} \mathcal{A}_q\mathcal{R}_q(t_R+\tau)e^{-i(qg\pi/2\sqrt{\bar{n}})}e^{-igq[\tau\sqrt{\bar{n}}+2\pi(c+2\bar{n})]}. \tag{25}$$

We first note that the rapidly oscillating phases are shifted in time by $2\pi(c+2\bar{n})/\sqrt{\bar{n}}$. This time shift does not affect the low frequency modulating terms $\mathcal{A}_q\mathcal{R}_q(t)$. Within the coherent state approximation, the overlap factors $\mathcal{R}_q(t_R+\tau)$ can be approximated by 1 for $|\tau| \lesssim 2\pi/g$. This means that, in the classical limit and within the coherent state approximation, close to the complete revival, the Rabi oscillation signal has the same fast oscillations than near $t=0$. This suggests to use Eqs. (23) and (24) as upper and lower envelopes. Because the Gea-Banacloche states are getting deformed over a time scale t_R, these expressions only provide an approximation to the real envelopes of the theoretical signal (25). This approximation assumes that the overlap factors $\mathcal{R}_q(t_R)$ do not depend on q. Because $|\mathcal{R}_q(t_R)-1|$ goes to zero as $1/\bar{n}$ in the large $\bar{n}$ limit, the accuracy of Eqs. (23) and (24) as approximate upper and lower envelopes for the main spontaneous resurgence increases with increasing $\bar{n}$.

To summarize, Eq. (23) describes the upper envelope of all revivals. The lower envelope is described by $P_-(t)$ in Eq. (22) for revivals involving only one frequency such as the ones occurring at $gt/2\sqrt{\bar{n}}=2\pi/q$ where $[N/2]<q\leq N$ and the lower envelope of the main revival which occurs at $gt/2\sqrt{\bar{n}}=2\pi$ is described by Eq. (24). In practice, only the lowest values of N ($N\leq 3$) may be easily reachable in the Rydberg atoms experiments and therefore, the only revival involving more than one value of $|m_+-m_-|$ is the complete one.

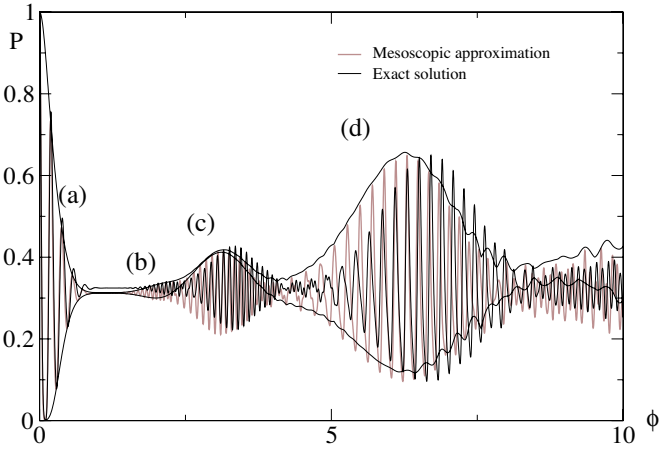

FIG. 5. (Color online) Spontaneous revivals of the Rabi oscillation signal $P=P_{m=J}$ for $N=3$ atoms ($J=3/2$), as a function of the dimensionless time $\phi=gt/2\sqrt{\bar{n}}$. The initial state $|m=3/2\rangle\otimes|\alpha\rangle$ with an average photon number $\bar{n}=|\alpha|^2=15$. The signal is computed using the mesoscopic approximation (gray line), its upper and lower envelopes (plain lines), and the exact solution (plain line with rapid oscillations) in the dissipationless case. Letters (a), (b), (c), and (d) refer to the overlaps of cavity field states for each revival depicted in Fig. 4. As expected, spontaneous revivals (b) and (c) are symmetric with respect to the flat signal and involve only one rapid frequency, respectively, given by $3g\sqrt{\bar{n}}$ and $2g\sqrt{\bar{n}}$.

3. Numerical results

All numerical results in this paper are presented in terms of the dimensionless time $\phi=gt/2\sqrt{\bar{n}}$ associated with the slow evolution induced by the atom + field interaction. Let us start by considering the case of the $N=1$ atom. Figure 2 shows the comparison between the analytic envelopes (22) and an exact numerical solution of the Schrödinger equation for different values of $\bar{n}$. As expected, the mesoscopic approximation becomes better and better as $\bar{n}$ increases. In this case, the upper and lower envelopes of the mesoscopic approximation signal are obtained by setting $q_r=1$ in Eq. (22).

Let us now consider the case of three atoms. Figure 5 presents a comparison between the results of an analytic exact diagonalization of the Tavis-Cummings Hamiltonian and the mesoscopic approximation. Correspondence with the revivals described in Fig. 4 is indicated. The upper and lower envelopes Eqs. (23) and (24) are depicted. Figure 5 shows that although the effective Hamiltonian does not fully reproduce the exact signal, it does reproduce the amplitude and the positions of the revivals in a satisfactory way.

As expected, Eqs. (23) and (24) effectively describe the upper and lower envelopes of the signal during the early collapse of Rabi oscillations. They fit also rather well with the first complete revival ($\phi\sim 2\pi$). But they fail for the re-

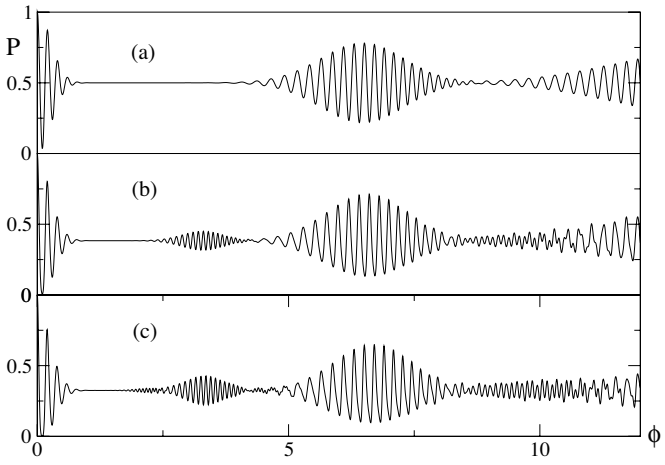

FIG. 6. Spontaneous revivals of the Rabi oscillation signal for $\bar{n}=15$, without dissipation, computed from a numerical integration of the Schrödinger equation for (a) $N=1$ atom, (b) $N=2$ atoms, (c) $N=3$ atoms as a function of the dimensionless time $\phi=gt/2\sqrt{\bar{n}}$. The initial condition is $m=N/2$ (all atoms excited).

vival at $\phi\sim\pi$: Eq. (23) corresponds to the upper envelope but Eq. (24) does not. This is not surprising since this revival is due to $q=2$. In this case, formulas (23) and (24) weigh the $q=2$ contribution with the same sign. Equation (22) with $q_r=2$ would be more appropriate to describe the envelopes near this revival.

Finally, the value $\mathcal{A}_0$ of the probability between revivals obtained from the effective Hamiltonian differs from the one obtained from the numerical solution of the Schrödinger equation in the case $N=3$. This is a finite $\bar{n}$ effect arising from the choice of the effective Hamiltonian (12). It can be checked that this difference vanishes as $\bar{n}^{-1/2}$ in the classical limit $\bar{n}\to+\infty$.

Comparing Rabi oscillation revival patterns at fixed $\bar{n}$ for various N shows that using two or three atoms instead of one induces an earlier spontaneous revival because the extreme Gea-Banacloche states ($m=\pm J$) move faster than the ones associated with $m=\pm 1/2$. But the weight of Rabi oscillations generated by high $|m|$ polarizations quickly decreases with N. Figure 6 suggests that the first spontaneous Rabi revival for $N=2$ and the second one for $N=3$ could be good candidates for the observation of spontaneous Rabi revivals. Of course, dissipation in the cavity leads to smaller Rabi oscillations as we shall see in the next section.

III. DISSIPATIVE DYNAMICS

A. Stochastic wave function approach to quantum dynamics

1. General principle

Within the context of cQED experiments performed with Rydberg atoms in microwave cavities, dissipation almost exclusively originates in cavity losses. They are extremely low since the quality factor Q of the cavity is of the order or higher than 10^8. Dissipation can be modeled through the coupling of the cavity mode to an harmonic bath with very short memory. Within this framework, the dynamics of the coupled atom + cavity system can be described by a master equation for its reduced density matrix. The master equation is valid over time scales much larger than the memory time τ_c of the bath. In the weak dissipation limit, which is realized here, it is still valid down to $T\simeq 0$ K and, in the present case, takes the form

$$\frac{d\rho}{dt}=-\frac{i}{\hbar}[H,\rho]+\gamma a\rho a^{\dagger}-\frac{\gamma}{2}(a^{\dagger}a\rho+\rho a^{\dagger}a), \qquad (26)$$

where H denotes the Tavis-Cummings Hamiltonian (3). Note that switching to an interaction representation for the atoms and the cavity mode does not modify the form of the dissipative terms and simplifies the Hamiltonian part. In principle, Eq. (26) can be solved numerically in order to obtain the quantum dynamics. However, an analytical ansatz for the reduced density matrix can be found within the mesoscopic approximation. As we shall see in the next section, this ansatz is conveniently derived using an alternative but equivalent approach to the dissipative dynamics of the atoms + cavity system: the quantum jump approach [10].

The basic idea underlying this approach is to consider that the environment of the system is continuously monitored so that any emission or absorption of quanta by the system can be assigned a precise date. Each time such an event occurs, the system undergoes a quantum jump. Between these jumps, its evolution is described by an effective Hamiltonian that describes both its intrinsic dynamics and the acquisition of information arising from the fact that no quanta has been detected. The probability rates for the various quantum jumps are directly obtained as averages of $L_i^{\dagger}L_i$ in the state under consideration where the L_i denote the quantum jump operator (here, only $L=\sqrt{\gamma}a$ is present at zero temperature). The reduced density matrix is then recovered by averaging over the set of stochastic trajectories associated with a large set of quantum jumps sequences. The weight of a given trajectory can be directly related to the dates and types of the various quantum jumps.

This method proves to be very convenient numerically since the number of variables involved is of the order of the dimension d of the system's Hilbert space whereas it scales as d^2 in the master equation approach. Note that the quantum jump approach is the only adequate formalism for studying the behavior of a single realization of the quantum system.

2. Decoherence of coherent state Schrödinger cats

Before applying this method to our problem, it is instructive to recall how the dissipative dynamics of an harmonic oscillator can be described in this way. In particular, we shall review how the decoherence scenario for a superposition of two coherent states can be recovered within this framework since it will prove to be useful in our cQED problem. At $T=0$ K, the system can only emit quanta. The stochastic dynamics of the quantum state is then described as follows.

During a small time interval $\tau\gg\tau_c$, the probability for a quantum jump is $p_{\tau}=\gamma\tau\langle\psi(t)|a^{\dagger}a|\psi(t)\rangle$ and the state after such a jump is $|\psi(t^+)\rangle=\sqrt{\gamma\tau}a|\psi(t)\rangle/\sqrt{p_{\tau}}$. Between jumps, the effective non-Hermitian Hamiltonian is given by

$$\hbar^{-1}H_{\text{eff}} = \omega_0 a^\dagger a - i\frac{\gamma}{2}a^\dagger a \tag{27}$$

and between t and $t+dt$ the state evolves according to

$$|\psi(t+dt)\rangle = \frac{(1-i\hbar^{-1}H_{\text{eff}}dt)|\psi(t)\rangle}{\sqrt{\Pi_0(t,dt)}}, \tag{28}$$

where the probability $\Pi_0(t,dt)$ that no quantum jump occurs between t and $t+dt$ is given, in the present situation, by $\Pi_0(t,dt)=1-p_{dt}$.

The evolution of a single coherent state $|\alpha\rangle$ is well known: apart from a well defined global phase factor, a quantum jump does not affect it. A coherent state remains coherent during the evolution between quantum jumps but its amplitude decreases exponentially due to the acquisition of information by negative measurements (no photon escapes) between the jumps $\alpha(t)=\alpha e^{i\omega_0 t-\gamma t/2}$.

Let us now consider a superposition of two distinct coherent states with the same average number of quanta $\bar{n}$ but with a relative phase θ in phase space

$$|\psi(0^-)\rangle = \frac{1}{\sqrt{2}}(|\alpha\rangle + |e^{i\theta}\alpha\rangle). \tag{29}$$

The jumps probability during time τ is then given by $p_\tau = \bar{n}\gamma\tau[1+2\,\text{Re}(\langle\alpha|\alpha e^{i\theta}\rangle e^{i\theta})]$ which simplifies to $\bar{n}\gamma\tau$ as soon as $|\alpha\rangle$ and $|\alpha e^{i\theta}\rangle$ are well separated so that their overlap can be safely neglected. Under this assumption, the state after a jump is given by

$$|\psi(0^+)\rangle = \frac{1}{\sqrt{2}}(e^{i\,\text{Arg}(\alpha)}|\alpha\rangle + e^{i[\text{Arg}(\alpha)+\theta]}|\alpha e^{i\theta}\rangle). \tag{30}$$

In the present unfolding of the master equation, each quantum jump introduces a phase factor $e^{i\theta}$ in the quantum superposition whereas each component remains a coherent state with the same parameter. Decoherence occurs because the number of jumps in a given time interval varies from one stochastic trajectory to the other. This has already been noticed in Ref. [18] using an unfolding of the master equation based on a continuous time measurement through a homodyne detection of the field leaving the cavity. The present scheme leads to the same final results but is more suited for our study of dissipation on the atoms + cavity dynamics.

Denoting by $\{t_1,\ldots,t_p\}$ the successive dates of quantum jumps $(0\le t_1<\cdots<t_p\le t)$, the final state associated with this sequence of jumps is given by

$$|\psi_{\{t_1,\ldots,t_p\}}(t)\rangle = \frac{1}{\sqrt{2}}(|\alpha e^{-\gamma t/2}\rangle + e^{ip\theta}|\alpha e^{-\gamma t/2}e^{i\theta}\rangle). \tag{31}$$

Thus, the decoherence coefficient is the characteristic function for the probability distribution of the number of quantum jumps $N[0,t]$ between 0 and t. The oscillator reduced density matrix at time t is given by

$$\rho(t) = |\alpha(t)\rangle\langle\alpha(t)| + |\alpha(t)e^{i\theta}\rangle\langle\alpha(t)e^{i\theta}| + \mathcal{D}(t)|\alpha(t)e^{i\theta}\rangle\langle\alpha(t)| + \mathcal{D}(t)^*|\alpha(t)\rangle\langle\alpha(t)e^{i\theta}|, \tag{32}$$

where $\mathcal{D}(t)$ denotes the average of $e^{iN[0,t]\theta}$ over all stochastic trajectories. When $\gamma t\gtrsim 1$, the reduction of the components amplitude has to be taken into account in order to get the probability distribution for a sequence of quantum jumps dates $0\le t_1\le\cdots t_p\le t$. This step is necessary to recover the full solution of the master equation (26). These computations are recalled in Appendix C. But for $t\ll\gamma^{-1}$, relaxation of energy has almost not occurred and we can assume that the average number of quanta in the two coherent components of the superposition is still equal to $\bar{n}$. Therefore, emission of quanta is a renewal process with a distribution of waiting times given by $\psi(\tau)=\bar{n}\gamma e^{-\bar{n}\gamma\tau}$. Decoherence by a sequence of quantum jumps obeying a renewal process has been recently studied in full generality [19]. In the present case, since $N[0,t]$ is distributed according to Poisson law with mean value $\bar{n}\gamma t$, the result is given by

$$\mathcal{D}(t) = \langle e^{iN[0,t]\theta}\rangle = \exp[\bar{n}\gamma t(e^{i\theta}-1)] \tag{33}$$

and leads to the same predictions as the direct solution of the master equation.

B. Decoherence in the mesoscopic approximation

Let us now turn to the dissipative dynamics in the atoms + cavity problem. Because Rydberg atom experiments are performed over time scales rather short compared to the dissipation time ($\gamma t\lesssim 0.1$), we shall look at the dissipative dynamics at short times when energy dissipation can be neglected ($\gamma t\ll 1$). In order to make an explicit connection with the work of Gea-Banacloche who has studied the effect of dissipation for one atom at arbitrary times [11], the case of longer times ($\gamma t\gtrsim 1$) is discussed in Appendix D. Let us finally mention that the case of an atomic ensemble has also been considered within the framework of master equation [20] which, in our opinion, does not clarify the dissipative quantum dynamics of the cavity + atoms system as much as the quantum stochastic trajectories method discussed below.

1. Evolution along a single stochastic trajectory

Inspired by the dissipationless case, we will focus on the evolution of factorized states of the form

$$|\Psi_m^X\rangle = \sum_{m''=-J}^{J} R^{-1}_{m'',m}|J,m''\rangle\otimes|\alpha\rangle, \tag{34}$$

which, within the mesoscopic approximation, remain factorized in the absence of dissipation. Strictly speaking, as noticed by Gea-Banacloche for $N=1$ and as proved in Appendix D, this is not true in the presence of dissipation. However, in the limit $\gamma t\ll 1$, the dissipative dynamics can still be formulated in terms of factorized states. Let us sketch the argument that justifies this assertion. We refer the reader to Appendix D for details.

Between quantum jumps, the state of the atoms + cavity system evolves according to Eq. (28) using the non-Hermitian Hamiltonian (27) which takes into account the information gained by observing that no quanta is emitted between two jumps. Because the atoms and the cavity mode are coupled, the whole atoms + cavity state should be af-

fected by this information gain. But, in the present strong coupling situation ($g \gg \gamma$), we expect the atoms to be mainly driven by the cavity and not by this indirect information gain. Next, dissipation induces an exponential decay of the average photon number $\bar{n}(t)=\bar{n}e^{-\gamma t}$ while keeping the photon number distribution Poissonian. We shall thus neglect the decay of $\bar{n}(t)$ for $\gamma t \ll 1$. The resulting evolution for the atoms + cavity case is the same as in the dissipationless case

$$|\Psi_m^X(t)\rangle \simeq e^{-igmt\sqrt{\bar{n}}}|D_m(t)\rangle \otimes |\psi_m(t)\rangle. \tag{35}$$

Let us now discuss the effect of a quantum jump on this state. Contrarily to coherent states, each Gea-Banacloche state $|\psi_m(t)\rangle$ does not remain invariant under the action of a quantum jump operator since

$$\begin{aligned} a|\psi_m(t)\rangle &= e^{-\bar{n}/2}\sum_{k=0}^{\infty} \alpha\frac{\alpha^k}{k!}e^{-igmt\sqrt{k+1}}|k\rangle \\ &= e^{-\bar{n}/2}\sum_{k=0}^{\infty} \alpha e^{imgt(\sqrt{k}-\sqrt{k+1})}\frac{\alpha^k}{k!}e^{-igmt\sqrt{k}}|k\rangle. \end{aligned} \tag{36}$$

The phase factor $\exp[imgt(\sqrt{k+1}-\sqrt{k})]$ *a priori* depends upon k. But expanding $\sqrt{k+1}-\sqrt{k}$ in powers of $(k-\bar{n})/\sqrt{\bar{n}}$ shows that, at first order, $\exp[imgt(\sqrt{k+1}-\sqrt{k})]$ is indeed independent of k. Using this approximation, the action of the annihilation operator reduces to the multiplication by a phase

$$a|\psi_m(t)\rangle \simeq \alpha e^{-imgt/2\sqrt{\bar{n}}}|\psi_m(t)\rangle. \tag{37}$$

It can be shown that an expansion to the next order differs from this expression by $O[(mgt/\bar{n})^2]$. Thus, Eq. (37) can be considered as a valid approximation in the domain $t \ll \sqrt{\bar{n}}/g$ which is in the domain of validity of the mesoscopic approximation ($t \ll \bar{n}/g$).

Let us now consider the evolution of state (34) along a single stochastic trajectory. Just before its first quantum jump, provided it happens at time t_1 such that $\bar{n}(t_1) \gg N$, we still have a factorized state of the form (35). The effect of a quantum jump occurring at time t_1 is to extract a phase $e^{i\theta_m(t_1)}$ where $\theta_m(t_1)$ is the argument of the amplitude of the quasicoherent state $|\psi_m(t_1)\rangle$. Iterating this argument shows that, in a stochastic trajectory with quantum jumps occurring at times $0 \le t_1 < \cdots < t_p \le t$, $|\Psi_m^X\rangle$ remains factorized but gets an extra phase $\theta_m(t_1,\ldots,t_p)$ associated with the quantum jumps

$$|\Psi_m^X\{t_1,\ldots,t_p\};t\rangle = e^{i\theta_m(t_1,\ldots,t_p)}e^{-igmt\sqrt{\bar{n}}}|D_m(t)\rangle \otimes |\psi_m(t)\rangle \tag{38}$$

and $\theta_m(t_1,\ldots,t_p)=\Sigma_j\theta_m(t_j)$. Exactly as for the case of a superposition of coherent states of an harmonic oscillator analyzed above, the accumulation of random relative phases in front of the Gea-Banacloche states leads to the decoherence of the Schrödinger cat state created by the strong atoms + cavity coupling and to the disappearance of Rabi oscillations.

Before discussing the average over all stochastic trajectories, it is worth mentioning that the present discussion remains valid even in the presence of the echo pulses introduced in Sec. II B. A π pulse instantaneously reverses the dynamics of the atoms + cavity system. After a single π pulse at time t_π, the Gea-Banacloche states invert their motion and start refocusing. The deterministic evolution of the atoms + cavity system is then described by a time-reversed evolution of the dissipationless motion. Therefore, the effect of any subsequent quantum jump is still to extract a phase corresponding to the position of the quasicoherent Gea-Banacloche state in the Fresnel plane at the jump time.

2. Average over stochastic trajectories

To deal with all these situations at once, let us denote by $\theta_m(t)$ the time-dependent phase of $|\psi_m(t)\rangle$, not assuming any particular form. The decoherence coefficient for the two states $|\Psi_{m_\pm}^X(t)\rangle$ considered here is thus given by the average over sequences of quantum jumps

$$\mathcal{F}[\theta_{m_+},\theta_{m_-}] = \langle e^{i\Sigma_l(\Delta\theta)(t_l)}\rangle, \tag{39}$$

where $(\Delta\theta)=(\theta_{m_+}-\theta_{m_-})(t)$ and the t_l are the dates of the successive quantum jumps occurring between 0 and t. This coefficient now depends in a functional way on the two trajectories $t \mapsto \theta_{m_\pm}(t)$ and should be called a decoherence functional in reference to the work of Feynman and Vernon [21]. Its definition (39) generalizes Eq. (33) to the case of a time dependent $\Delta\theta$. Since we assumed that $\gamma t \ll 1$, the statistics of waiting times between quantum jumps is independent of the positions of the Gea-Banacloche states. Exactly as in Sec. III A 2, it is given by $\psi(\tau)=\bar{n}\gamma e^{-\bar{n}\gamma\tau}$. Within this approximation, Eq. (39) can be computed explicitly even for a time dependent $\Delta\theta$. An elegant way to get the result consists into rewriting the sum over the number of quantum jumps in a completely different way which does not singularize any specific time

$$\mathcal{F}[\theta_{m_+},\theta_{m_-}] = \left\langle \prod_{0\le t'\le t}[1+n(t')(e^{i(\Delta\theta)(t')}-1)]\right\rangle, \tag{40}$$

where $n(t')=0$ if no event occurs at time t' and $n(t')=1$ when a quantum jump occurs at time t' and $(\Delta\theta)=\theta_{m_+}-\theta_{m_-}$. Note that in the above expression, t' is not the time of a quantum jump. The formal infinite product in the r.h.s of (40) can then be expanded leading to an expansion involving multitime correlators $\langle n(t_1')\cdots n(t_r')\rangle$, where $0 \le t_1' \le \cdots \le t_r' \le t$ (here, r is not the number of quantum jumps). Because $n(\tau)=0$ or 1:

$$\langle n(t_1')\cdots n(t_r')\rangle = \langle n(t_1')\rangle \prod_{l=1}^{r-1} \mathrm{P}(t_{l+1}'|t_l'), \tag{41}$$

where $\mathrm{P}(t_{l+1}'|t_l')=\mathrm{Prob}[n(t_{l+1}')=1\,|\,n(t_l')=1]$. At short times, quantum jumps provide a renewal process and therefore the conditional probabilities $\mathrm{P}(t_{l+1}'|t_l')$ are directly related to the average density of jumps $S(t)$: $\mathrm{P}(t_{l+1}'|t_l')=S(t_{l+1}'-t_l')$. Moreover, $\langle n(t_1')\rangle = S(t_1')$. Here the density of events is a constant: $S(t)=\gamma\bar{n}$. The final result for the decoherence functional is thus

$$\mathcal{F}[\theta_{m_+},\theta_{m_-}] = \exp\left(\gamma,\bar{n}\int_0^t (e^{i(\Delta\theta)(\tau)}-1)d\tau\right). \quad (42)$$

Finally, expression (42) can be interpreted as resulting from the accumulation of decoherence coefficients over infinitesimal periods of time. In the mesoscopic regime, because of the strong coupling regime, the evolution of the atoms + cavity system is a forced evolution of the cavity state driven by the atomic polarizations $|D_m(t)\rangle$, leading to the motion of the Gea-Banacloche states $|\psi_m(t)\rangle$. For each Gea-Banacloche state, this forced motion between τ and $\tau+d\tau$ leaves an imprint in the environment of the cavity. The overlap between imprints left by two distinct Gea-Banacloche states is precisely the decoherence coefficient. During infinitesimal time $d\tau$, the imprint left in the environment by each Gea-Banacloche state under consideration is the same as the one left by coherent states with the same average number of quanta but a time-dependent phase separation $(\Delta\theta)(\tau)$. Therefore, the corresponding decoherence coefficient is given by

$$D(\tau,\tau+d\tau) \simeq \exp[\gamma\bar{n}(e^{i(\Delta\theta)(\tau)}-1)d\tau]. \quad (43)$$

Since the environment is Markovian, the infinitesimal decoherence coefficients (43) associated with different time windows $[t,t+\tau]$ $(\tau \gg \tau_c)$ accumulate through time evolution, leading to Eq. (42).

C. Rabi oscillations in the presence of dissipation

1. Spontaneous revivals

It is now straightforward to compute the Rabi oscillation signals by introducing the decoherence coefficients for all pairs of Gea-Banacloche states that can appear in the reduced atomic density operator. Because we are dealing with experimental situations such that the duration of experiment is small compared to the cavity dissipation time, we shall assume that the average number of quanta remains equal to $\bar{n}$ in this paragraph and the following ones.

The result for the Rabi oscillation signal is $(q=m_+-m_-)$

$$P_m(t) = \sum_{m_+,m_-} e^{-igqt\sqrt{\bar{n}}/2}\mathcal{P}_{m_+,m_-}(t)\mathcal{R}_{m_+,m_-}(t)\mathcal{F}_{m_+,m_-}(t), \quad (44)$$

where $\mathcal{P}_{m_+,m_-}(t)$ and $\mathcal{R}_{m_+,m_-}(t)$, are respectively, given by Eqs. (18) and (20). Decoherence is contained in $\mathcal{F}_{m_+,m_-}(t) = e^{-d_q(t)+i\Theta_q(t)}$ which can be evaluated using Eq. (42), thus leading to $(\phi=gt/2\sqrt{\bar{n}})$

$$d_q(t) = \frac{2\gamma\bar{n}^{3/2}\phi}{g}\left(1-\frac{\sin(q\phi)}{q\phi}\right), \quad (45)$$

$$\Theta_q(t) = \frac{4\gamma\bar{n}^{3/2}}{gq}\sin^2\left(\frac{q\phi}{2}\right). \quad (46)$$

Note that in these results, $\bar{n}^{3/2}\gamma/g$ is the dimensionless parameter that characterizes the strength of decoherence. An ansatz for the upper and lower envelopes of the Rabi oscillation signal in the presence of dissipation can then be obtained along the lines of Sec. II D 2

$$P_+(t) = \mathcal{A}_0 + \sum_{q\neq 0}|\mathcal{R}_q(t)\mathcal{A}_q|e^{-d_q(t)}, \quad (47)$$

$$P_-(t) = \mathcal{A}_0 + \sum_{q\neq 0}(-1)^q|\mathcal{R}_q(t)\mathcal{A}_q|e^{-d_q(t)}. \quad (48)$$

2. Induced revivals

Rabi oscillation signals in an echo experiment can also be computed within the mesoscopic approximation. The percussional echo pulse is applied to the atoms at time t_π. It corresponds to the operator $U_\pi=\otimes_{j=1}^N\sigma_j^z$. Using this operator, Eq. (9) can be derived for the case of N atoms with H_{TC} in place of the Jaynes-Cummings Hamiltonian. Thus, exactly as for $N=1$, the evolution of the atoms + cavity system is reversed after time t_π. Within the mesoscopic approximation, this means that atomic polarization as well as Gea-Banacloche states move backward towards their initial positions. The time dependence of the associated phases $\theta_m(\tau)$ associated with Gea-Banacloche states is given by

$$\begin{aligned}\theta_m(\tau) &= mg\tau/2\sqrt{\bar{n}} \quad \text{for } 0\leq\tau\leq t_\pi,\\ \theta_m(\tau) &= mg(2t_\pi-\tau)/2\sqrt{\bar{n}} \quad \text{for } t_\pi\leq\tau.\end{aligned} \quad (49)$$

Equation (42) leads to the following decoherence coefficient $(t\geq t_\pi)$ which we write as $\mathcal{F}^{(\text{echo})}_{m_+,m_-}(t_\pi,t)=e^{-d_q(t_\pi,t)+i\Theta_q(t_\pi,t)}$ where $(q=m_+-m_-)$:

$$d_q(t_\pi,t) = \frac{2\gamma\bar{n}^{3/2}}{g}\left(\phi-\frac{2\sin(q\phi_\pi)-\sin(q(2\phi_\pi-\phi))}{q}\right), \quad (50)$$

where $\phi_\pi=gt_\pi/2\sqrt{\bar{n}}$ and

$$\Theta_q(t_\pi,t) = \frac{4\gamma\bar{n}^{3/2}}{gq}\{2\sin^2(q\phi_\pi/2)-\sin^2[q(2\phi_\pi-\phi)/2]\}. \quad (51)$$

Because of the perfect time reversal for the atoms + cavity system, the overlap factor $\mathcal{R}_{m_+,m_-}$ in the echo experiment can be expressed in terms of the overlap factor under free evolution for $t\geq t_\pi$: $\mathcal{R}^{(\text{echo})}(t_\pi,t)=\mathcal{R}(2t_\pi-t)$.

3. Extension to finite temperature

It is known that increasing the temperature lowers the decoherence time. For the harmonic oscillator, initially in a coherent state, the exact solution to the quantum master equation (26) is well known [22]. At time t, the state is no longer pure but appears to be a thermal state with average number of quanta $\bar{n}(t)=\bar{n}_T(1-e^{-\gamma t})$ translated in phase space by $\alpha e^{-\gamma t/2}$ ($\bar{n}_T$ denoting the average number of quanta at equilibrium at temperature T). Nevertheless for times much shorter than dissipation, thermalization can be neglected: the state of the oscillator can still be considered as coherent. The analysis of the solution of the master equation at finite tem-

peratures shows that decoherence at short times is still exponential. The effect of temperature is to enhance the damping rate by a factor $2n_{\mathrm{th}}+1=\coth(\beta\hbar\omega_0/2)$. This suggests that the imprint of the superposition of two coherent states in the environment during an infinitesimal time interval $d\tau$ at finite temperature is obtained by substituting $\gamma \rightarrow \gamma\coth(\beta\hbar\omega_0/2)$ in Eq. (43). Following the previous line of reasoning (end of Sec. III B 2), the decoherence coefficient at time t for a superposition of two coherent states is again obtained by summing the decoherence coefficients associated with infinitesimal time intervals between $\tau=0$ and $\tau=t$.

This result can be used to derive the evolution of the atoms + cavity density matrix at short times and moderate finite temperature. As long as we can neglect the thermalization, the only effect of dissipation is to damp the coherences between states $|D_{m_\pm}(t)\rangle\otimes|\psi_{m_\pm}(t)\rangle$ for $m_+\neq m_-$. As in the zero temperature case, each of the state $|D_{m_\pm}(t)\otimes|\psi_{m_\pm}(t)\rangle$ is expected to evolve according to the atoms + cavity interaction and the echo pulse applied to the system (if any). As explained in the previous paragraph, the decoherence coefficient $\mathcal{F}_{m_+,m_-}(t)$ to be used in Eq. (44) is obtained by replacing γ by $\gamma\coth(\beta\hbar\omega_0/2)$ in Eqs. (45), (46) for the free evolution and Eqs. (50), (51) for the echo experiment. Note that this ansatz is expected to be valid only for low temperatures and at short times such that $\gamma t\coth(\beta\hbar\omega_0/2)\ll 1$.

IV. DISCUSSION OF THE RESULTS

A. Method and parameters

We have considered the Rabi oscillation signal in the presence of dissipation for $N=1$ to $N=3$ atoms, values that can be realistically reached in state-of-the-art cavity QED experiments. Photon numbers $\bar{n}=10$ and 15 have been considered. All our computations have been performed for values of g/γ corresponding to the present ENS experiment [4]. The best published cavity damping time is 1 ms (quality factor $Q=3.2\times10^8$). Preliminary tests of an improved experimental setup have shown damping rates of 14 ms ($Q=4.5\times10^9$) and even 115 ms ($Q=3.7\times10^{10}$) and these results are to be submitted in the near future. Thus, the values of 14 ms ($g/\gamma\simeq4310$), 5 ms ($g/\gamma\simeq1540$ and $Q=1.6\times10^9$) and 1 ms ($g/\gamma\simeq308$) for the damping rate of the cavity have been considered in our simulations. We focus on the case of a zero-temperature bath which can be realistically reached as shown in [23]. The effect of finite temperature will be briefly discussed in Sec. IV D.

Results of the analytical approach described in Sec. III C have been compared to a quantum Monte Carlo simulation of the atoms + cavity system evolution in the spirit of Ref. [10]. For these simulations, the Adams-Bashford scheme of order four has been used to compute the evolution of the wave function between quantum jumps.

We first present our results relative to the free evolution of the atoms + cavity (spontaneous Rabi oscillations revivals) in Sec. IV B and for the echo experiments in Sec. IV C. Consequences of these results for cQED and circuit-QED experiments are then discussed in Sec. IV D 2.

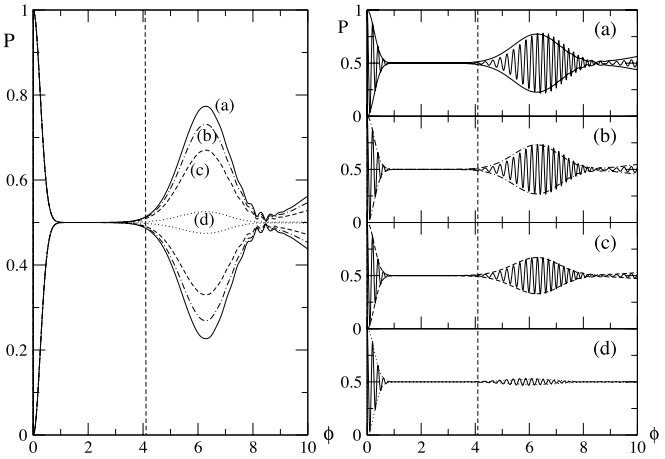

FIG. 7. Influence of dissipation on the spontaneous revivals of the Rabi oscillation signal $P=P_{m=J}$ (as a function of $\phi=gt/2\sqrt{\bar{n}}$) for one atom and $m=1/2$ (atom excited) with $\bar{n}=15$ photons initially. The graph on the left depicts the analytical envelopes $P_\pm(t)$ for (a) no dissipation, (b) $\gamma^{-1}\simeq14$ ms, (c) $\gamma^{-1}\simeq5$ ms, and (d) $\gamma^{-1}\simeq1$ ms. The right part of the figure presents the associated Rabi oscillation signals obtained from quantum Monte Carlo simulations (plain lines) as well as the associated analytical envelopes. The vertical dashed line corresponds to the largest reachable ϕ (atoms at 100 m s^{-1}).

B. Free evolution

It is interesting to assess the possibility of observing spontaneous Rabi oscillation revivals, since, for $N>1$, such a revival might be observable at shorter times than in the $N=1$ case. Figure 7 presents a comparison between the Rabi oscillation signals resulting from the interaction with a mesoscopic coherent state containing 15 photons in average in the dissipationless case and for dissipation times equal to 1, 5, and 14 ms ($T=0$ K). Figures 8 and 9 present the same comparison for the cases of $N=2$ and $N=3$ atoms, respectively. Note that our analytical model [Eqs. (47) and (48)] predicts the upper and lower envelopes of the Rabi oscillation signal with a rather good precision in the presence of dissipation. Note that in the $N=1$ case, this simulation shows that it is not possible to observe spontaneous Rabi oscillation revivals with the present cavity ($\gamma\lesssim1$ ms). The same conclusion is valid for $N=2$ and $N=3$: even the partial revivals that occur before the main one $\phi\sim2\pi$ should not be observable. For $\gamma^{-1}=1$ ms, decoherence transforms the entangled atom + cavity state into a statistical mixture before any pair of Gea-Banacloche components of the field overlap. As Figs. 7–9 show, improving the quality factor of the cavity could enable a direct observation of the spontaneous revivals in the presence of $\bar{n}=15$ photons.

However, the experimental apparatus sets a tight limitation on the interaction time of the atoms with the cavity field. The number of atoms flying through the apparatus at velocities lower than 100 m s^{-1} is too small in a thermal atomic beam to be used in practice. Atomic spontaneous emission is another limitation for very slow atoms. We stick here to the available apparatus and set an upper limit on ϕ which could roughly be estimated as $\phi_m\simeq2\pi(2.5/\sqrt{\bar{n}})$. This upper limit

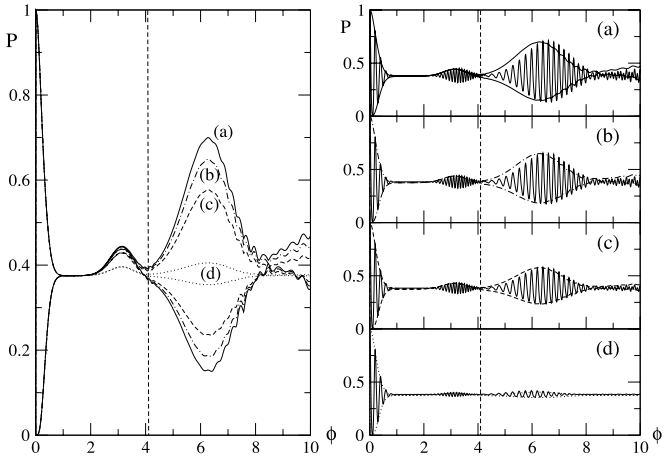

FIG. 8. Influence of dissipation on the spontaneous revivals of the Rabi oscillation signal $P=P_{m=J}$ (as a function of $\phi=gt/2\sqrt{\bar{n}}$) for $N=2$ atoms. The initial condition is $m=1$ (all atoms excited) with $\bar{n}=15$ photons. The graph on the left depicts the analytical envelopes $P_{\pm}(t)$ for (a) no dissipation, (b) $\gamma^{-1}\simeq 14$ ms, (c) $\gamma^{-1}\simeq 5$ ms, and (d) $\gamma^{-1}\simeq 1$ ms. The right part of the figure presents the associated Rabi oscillation signals obtained from quantum Monte Carlo simulations (plain lines) as well as the associated analytical envelopes.

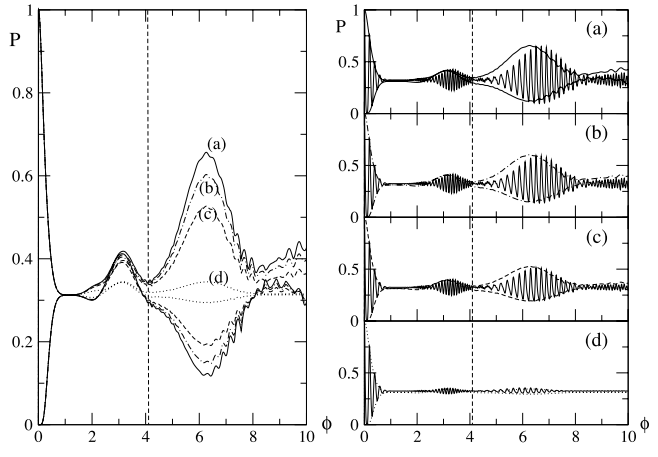

FIG. 9. Influence of dissipation on the spontaneous revivals of the Rabi oscillation signal $P=P_{m=J}$ (as a function of $\phi=gt/2\sqrt{\bar{n}}$) for $N=3$ atoms. The initial condition is $m=3/2$ (all atoms excited) with $\bar{n}=15$ photons. The graph on the left depicts the analytical envelopes $P_{\pm}(t)$ for (a) no dissipation, (b) $\gamma^{-1}\simeq 14$ ms, (c) $\gamma^{-1}\simeq 5$ ms, and (d) $\gamma^{-1}\simeq 1$ ms. The right part of the figure presents the associated Rabi oscillation signals obtained from quantum Monte Carlo simulations (plain lines) as well as the associated analytical envelopes.

for $\phi/2\pi$ ranges from 0.65 ($\bar{n}=15$) to 0.76 ($\bar{n}=10$) which excludes the observation of the complete revival obtained when all Gea-Banacloche states overlap again. Nevertheless, as can be seen from graphs (b) and (c) in Figs. 8 and 9, observing a spontaneous partial revival may be possible for $N=2,3$. In the case of two atoms, the signal would correspond to the overlap of states $|\psi_1\rangle$ and $|\psi_{-1}\rangle$. In the case of three atoms, the signal would be dominated by two overlaps corresponding to $|\psi_{1/2}\rangle$ and $|\psi_{-3/2}\rangle$ on one side and $|\psi_{-1/2}\rangle$ and $|\psi_{3/2}\rangle$ on the other side. Note that the partial revival associated with the overlap between $|\psi_{3/2}\rangle$ and $|\psi_{-3/2}\rangle$ is not within reach. Observing a spontaneous revival requires $\phi\simeq\pi$ to remain within reach for the slowest atoms. This puts an upper limit on the average photon number close to 25 photons.

Finally, Fig. 10 shows the decay of the modulus of the three decoherence coefficients $\mathcal{F}_q(t)$ as a function of time for $\bar{n}=10$ and $\bar{n}=20$ for dissipation times equal to 1, 5, and 14 ms. It clearly shows that, even if the time of flight problem could be circumvented, increasing the number of photons puts strong constraints on the dissipation time of the cavity. This suggests that working with 10 to 15 photons in average is a good compromise for observing spontaneous partial revivals.

C. Echo experiment

In this paragraph, results for the simulation of an echo experiment corresponding to an echo pulse at $t_\pi=30$ μs are presented. Figure 11 shows the simulated echo signals for the cQED experiment at LKB obtained with 15 photons initially and an echo pulse at 30 μs for $N=1$, 2 and 3 atoms and two different values of dissipation: 14, 5, and 1 ms. Note that in the case of three atoms, a revival occurs at 150 μs. It corresponds to a delayed revival of type (c) in Fig. 4. But although its amplitude makes it visible with a 14 ms dissipation time, the time of flight limitation will prevent it from being observed in the experiment. The same conclusion holds for the delayed revival predicted also in the $N=2$ atoms case.

D. Finite temperature

1. Thermalization procedure

Experiments with Rydberg atoms in high-quality microwave cavities are performed at low temperatures ($T\simeq 0.8-1.4$ K). In order to wash out photons resulting from thermal

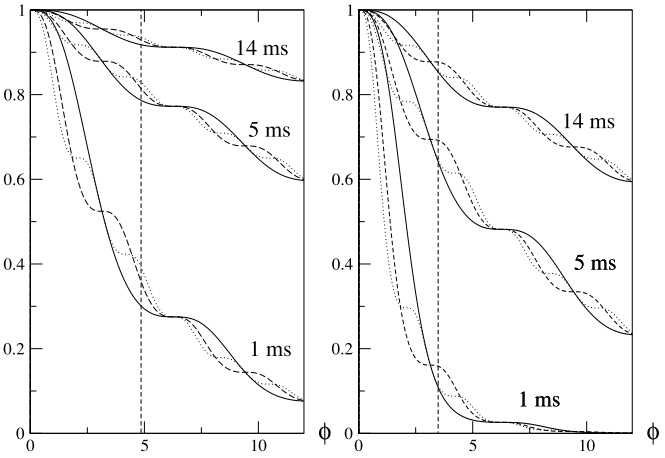

FIG. 10. Modulus of the decoherence coefficient $\mathcal{F}_q(t)$ for $q=1$ (plain lines), $q=2$ (dashed lines), and $q=3$ (dotted lines) as a function of ϕ for dissipation times 14, 5, and 1 ms in the case of $\bar{n}=10$ photons (left graph) and $\bar{n}=20$ photons (right graph). The vertical dashed line corresponds to the largest reachable ϕ (atoms at 100 m s^{-1}).

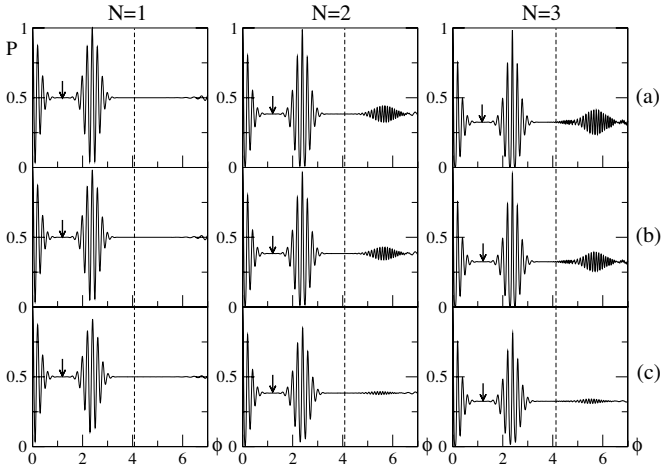

FIG. 11. Echo signal (function of $\phi = gt/2\sqrt{\bar{n}}$) simulated for $\bar{n} = 15$ at $t_\pi = 30$ μs and $g/2\pi = 49$ kHz. All graphs on a row correspond to the same dissipation time (a) $\gamma^{-1} = 14$ ms, (b) $\gamma^{-1} = 5$ ms, and (c) $N = 3$ and $\gamma^{-1} = 1$ ms. All graphs in a column correspond to the same number of atoms. The arrow shows the time of the echo pulse. The vertical dashed line corresponds to the largest reachable ϕ value (slowest atoms at 100 m s^{-1}). The initial condition is $m = 3/2$ (all atoms excited).

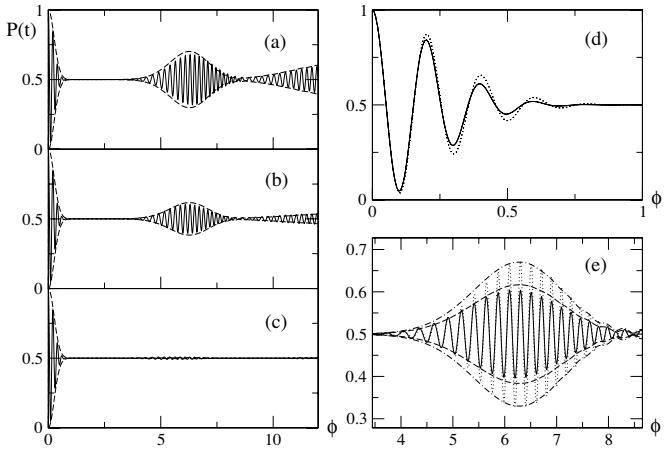

FIG. 12. Rabi oscillation signals obtained from quantum Monte Carlo simulations for one atom using the thermalization protocol producing a thermal state with 0.15 photons displaced in Fresnel plane by an amplitude corresponding to $\bar{n} = 15$ photons, for (a) $\gamma^{-1} = 14$ ms, (b) 5 ms, and (c) 1 ms. Graph (d): comparison between zero temperature signals (dashed line) and finite temperature signals (full line) at short times for $\gamma^{-1} = 5$ ms. Graph (e): comparison between zero temperature signals (full line) and finite temperature signals (dotted line) for $\gamma^{-1} = 5$ ms. Dashed lines represent the upper and lower envelopes $P_\pm$ obtained by taking temperature into account by rescaling $\gamma \mapsto (1 + 2n_{\text{th}})\gamma$.

leaks, an erasing procedure using auxiliary atomic samples is applied [1]. Once the erasing procedure has been completed, a coherent field is injected inside the cavity. Because of the imperfections of the procedure and because of the necessary delay $\tau_1 \simeq 200$ μs between the erasing sample and the coherent field injection, this creates a translated thermal state, partially thermalized. This state would then evolve during time $\tau_2 \simeq 50$ μs before the experimental atomic sample enters the cavity.

In order to model this preparation, we have performed a quantum Monte Carlo simulation involving a finite temperature environment and an initial thermalization period of duration t_p. At the beginning of this preparation period, a coherent state is injected in the dissipative cavity and evolves decoupled from the atoms during time t_p. Then the coupling to the atoms is turned on to model the experiment. A rather pessimistic estimate of the average number of thermal photons per mode of the reservoir has been used for this simulation ($n_{\text{th}} \simeq 0.4$ corresponding to $T \simeq 2$ K at 51 GHz). It has been estimated that thermal fluctuations left by the imperfect erasure procedure correspond to at most $n_0 \simeq 0.15$ photons per mode on the average. Using $n_0 = n_{\text{th}}(1 - e^{-\gamma t_p})$, this sets $\gamma t_p \simeq 0.47$ used in our numerical thermalization protocol. The injected coherent state before thermalization has an amplitude $\alpha_0 = \sqrt{\bar{n}} e^{\gamma t_p/2}$ in order to take into account the exponential decay during the preparation phase ($\bar{n}$ denotes the average photon number when the experimental atomic sample is injected inside the cavity).

2. Finite temperature results

Figure 12 presents the results of these simulations for $N = 1$ atom. The main curve presents the Rabi oscillation signals obtained from a quantum Monte Carlo simulation implementing the thermalization procedure described above for $\gamma^{-1} = 1$, 5, and 14 ms. In order to compare it with the analytical model we have used the fact that, in the present case, at times short compared to the dissipation time, the main effect of finite temperature is to speed up decoherence. This is taken into account by replacing γ by $\gamma(1 + 2n_{\text{th}})$ in the decoherence functional [Eqs. (45) and (46)]. This ansatz is used to compute the upper and lower envelopes that appear in Fig. 12.

Note that some features are not reproduced by our analytical ansatz since the overlap factor we use does not take into account thermalization of the quasicoherent state $|\psi_m(t)\rangle$. As shown in graph (d), the initial collapse of Rabi oscillations occurs earlier than at zero temperature. On the other hand, the envelope of the spontaneous revival is well described by our model [see graph (e)]. This shows that our analytical approach is quite efficient in predicting the contrast of spontaneous revivals of the Rabi oscillation signals even at finite temperature.

Results for the case of three atoms are presented on Fig. 13. The same effects as for $N = 1$ can be observed here. Note that thermal fluctuations do reduce the contrast of spontaneous revivals albeit not enough to make them unobservable for $\gamma^{-1} = 5$ and 14 ms. As shown in graph (e), thermal effects reduce the contrast of the main secondary revival from 15 to 11 % for 5 ms dissipation time. As mentioned above, improving the dissipation time reduces the impact of thermalization.

E. Discussion of the results

1. Perspectives for the ENS experiment

Within the context of cQED experiments performed at ENS, our results suggests that spontaneous revivals of Rabi

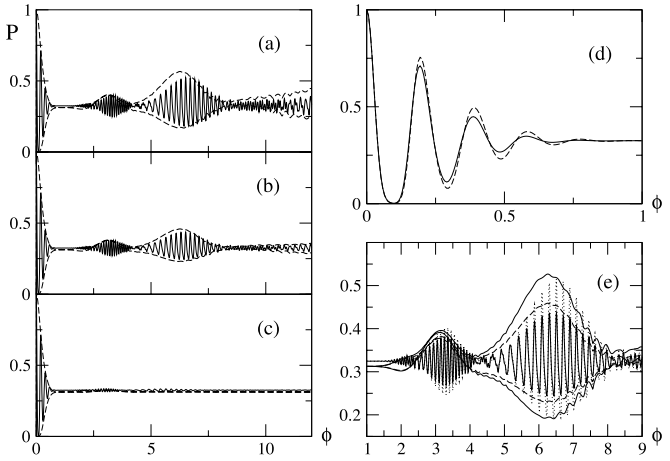

FIG. 13. Rabi oscillation signals obtained from quantum Monte Carlo simulations for $N=3$ atoms using the thermalization protocol producing a thermal state with 0.15 thermal photon number displaced in Fresnel plane with $\bar{n}=15$ for (a) $\gamma^{-1}=14$ ms, (b) 5 ms, and (c) 1 ms. Graph (d): comparison between zero temperature signals (dashed line) and finite temperature signals (full line) at short times for $\gamma^{-1}=5$ ms. Graph (e): comparison between zero temperature signals (full line) and finite temperature signals (dotted line) for $\gamma^{-1}=5$ ms. Dashed lines represent the upper and lower envelopes $P_{\pm}$ obtained by taking temperature into account by rescaling $\gamma \mapsto (1+2n_{\mathrm{th}})\gamma$.

oscillations could be observed in an improved experimental setup with two or three atoms and an initial coherent state containing from 10 to 15 photons on the average. A convincing test of the generation of three- and four-component Schödinger cat states involving 10 photons and two or three atoms would require to probe the phase distribution using a homodyne method [3]. The splitting of the initial state into $N+1$ separated phase peaks followed by the recombination of some of them at the time of partial spontaneous revivals would provide an experimental proof of the scenario presented in the present paper. A more detailed insight into the field dynamics could be gained by reconstructing the cavity field Wigner function, using the method proposed by and Davidovich and already implemented on a one-photon field in Ref. [24].

2. Experimental consequences for circuit QED experiments

Our analysis can be used to discuss the case of circuit-QED experiments [12]. Of course, our model does not take into account relaxation nor dephasing of the atoms themselves, since they are not relevant for the Rydberg atom experiments. In the case of circuit QED, the relaxation and decoherence of Josephson qubits must be taken into account to obtain a precise model of the dissipative dynamics. In the literature, the g/γ ratio is around 20 [25,26]. Therefore, our model suggests that observing the effects discussed in the present paper in circuit QED experiments requires an improvement of roughly two orders of magnitude on this ratio.

Increasing g/γ would then require either an increase of the resonator quality factor or an increase of the qubit/cavity coupling. Using classical eletrodynamics, an upper bound on the value of g can be estimated to be of the order of $g/\omega_0 \simeq \Lambda\sqrt{2\alpha/\epsilon_r}$ where α is the fine structure constant, ϵ_r the relative permittivity of the substrate and Λ collects geometrical form factors and capacitance ratios determining the microstrip impedance and its coupling to the qubit. For resonators in the 1–10 GHz frequency range, values of $g/2\pi$ of the order of 100 MHz are quite realistic and would already provide a factor 5 on g/γ. In present circuit-QED experiments, detection is performed by probing the cavity through transmission measurements. This requires lowering the quality factor from 10^6 [27] to 10^4 which is still in the strong coupling regime but not as deeply as for Rydberg atom experiments. Less dissipative cavities could then be used provided one could improve the qubits properties or use an alternative measurement method. Recently, new detection schemes based on dynamical bifurcation of Josephson junctions have been developed and provide high contrast, rapid measurement, low back action and absence of on-chip dissipation [28–30]. Thus, although important progress is required for circuit-QED devices, the rapid improvement of Josephson device technology is very encouraging and provides a strong motivation for further theoretical studies.

V. CONCLUSION

We have studied the resonant interaction of an ensemble of N atoms symmetrically coupled to a resonant mesoscopic field in a cavity. The interaction between the atomic ensemble and the cavity produces an entangled state with $N+1$ components leading to a rich pattern for Rabi oscillation revivals that generalizes the ones obtained in the $N=1$ case. In particular, "fractional" spontaneous revivals reflecting partial disentanglement of the atom + cavity state are expected to occur earlier than the first spontaneous revival in the $N=1$ case.

Dissipation in the cavity will lead to decoherence of this mesoscopic entangled state and we have proposed a simple analytical model that enables us to compute the Rabi oscillation signals in the presence of dissipation. This model provides simple expressions for the spontaneous Rabi oscillations revivals as well as for the ones induced in an echo experiment. Analytical results are in good agreement with quantum Monte Carlo simulations and provide an intuitive view of the evolution of the dissipative atoms+ cavity system. We have obtained an analytical expression for the accumulated decoherence of the $N+1$-component Schrödinger cat state resulting from the atom +field interaction which could be used for tests of decoherence.

We have shown that in a forthcoming generation of cQED experiments, spontaneous revivals of Rabi oscillations associated with the recombination of a fraction of the $N+1$ components of the entangled atoms + cavity state should be observable. An improvement by a factor 10 in the cavity quality factor as well as the use of slow atoms (100 m/s) are required. Our analysis also suggests that the situation is not so favorable within the context of circuit-QED experiments, due to the measurement limited quality factor. However, rapid progress in this field is extremely encouraging and motivates further theoretical studies taking into account relax-

ation and dephasing of the qubits. The stochastic wave function approach could be used to take these dissipative phenomena into account at least for the part due to high frequency noise. Dissipative dynamics in the presence of a strong low frequency $1/f$ noise cannot be accounted for within the framework of the Bloch-Redfield equations [31]. Nevertheless, providing a simple analytical model for the dissipative dynamics of a combined qubits + cavity system taking into account all possible sources of dissipation would be an interesting challenge.

ACKNOWLEDGMENTS

We thank P. Bertet and O. Buisson for useful discussions on forthcoming progress in Josephson device technology.

APPENDIX A: MESOSCOPIC APPROXIMATION

In the classical limit, we expect eigenstates of J^x to remain unentangled with the cavity state. Therefore, let us start from an initial state

$$|\Psi_m^X\rangle = \sum_{m''=-J}^{J} R^{-1}_{m'',m}|J,m''\rangle \otimes |\alpha\rangle, \tag{A1}$$

where $\alpha=\sqrt{\bar{n}}$ and $R_{m,m'}=\langle J,m'|e^{i\pi J^y}|J,m\rangle$. Since we are in the mesoscopic regime, most of the weight of the state is concentrated in stable subspaces $\mathcal{H}_n$ with n close to $\bar{n}$. Apart from the term $m'=J$, the above sum also spreads on the lower dimensional stable subspaces. Since we expect this contribution to be exponentially weak in the mesoscopic domain, we focus the projection $|\tilde{\Psi}_m^X\rangle$ of $|\Psi_m^X\rangle$ in $\oplus_n\mathcal{H}_n$. Because the effective Hamiltonian (12) is written in terms of the $\mathcal{J}^x$ generator, it is useful to decompose $|\Psi_m^X\rangle$on the basis vectors $|X_m^{(n)}\rangle$. We start from

$$|\tilde{\Psi}_m^X\rangle = e^{-\frac{\bar{n}}{2}}\sum_{k,m'} \frac{\bar{n}^{k/2}}{\sqrt{k!}} R^{-1}_{m,m'}|Z_{m'}^{(k-J+m')}\rangle, \tag{A2}$$

where the sum over k ranges from $J-m'\geq 0$ to $+\infty$. Shifting the index k into $p=k+m'-J\geq 0$ and approximating $\sqrt{\bar{n}^k/k!}$ by $\sqrt{\bar{n}^p/p!}$ enables us to do the summation over m' using $|Z_m^{(p)}\rangle=\Sigma_{m''}R_{m,m''}|X_{m''}^{(p)}\rangle$. This finally leads to

$$|\tilde{\Psi}_m^X\rangle \simeq e^{-\bar{n}/2}\sum_{p=0}^{\infty} \frac{\alpha^p}{\sqrt{p!}}|X_m^{(p)}\rangle. \tag{A3}$$

When evolved during time t under the effective Hamiltonian (12), this state becomes

$$|\tilde{\Psi}_m^X(t)\rangle = e^{-\frac{\bar{n}}{2}}\sum_{p=0}^{\infty} \frac{\alpha^p}{\sqrt{p!}} e^{-igtm\sqrt{p+c}}|X_m^{(p)}\rangle. \tag{A4}$$

We now use the R^{-1} matrix to go back to the usual basis $|X_m^{(p)}\rangle=\Sigma_{m'}R^{-1}_{m,m'}|Z_{m'}^{(p)}\rangle$. In order to rewrite the resulting state as a tensor product of an atomic polarization and a field state, it is necessary to introduce the same approximations as before. We first approximate $\sqrt{(p+l)!/p!}\,\bar{n}^p\sim 1$. The coefficient of $|J,J-l\rangle\otimes|p+l\rangle$ is then equal to

$$\frac{\bar{n}^{(p+l)/2}}{\sqrt{(p+l)!}} R^{-1}_{m,J-l} e^{-igmt\sqrt{p+c}}.$$

We then replace $e^{-igmt\sqrt{p+c}}$ by $e^{-igmt\sqrt{p+l}}$ multiplied by the phase factor $e^{igmt(\sqrt{p+l}-\sqrt{p+c})}$. This last phase factor is then expanded to first order near $\bar{n}$ which leads to a slowly varying phase $e^{igmt(l-c)/2\sqrt{\bar{n}}}$. The resulting coefficient now only depends on l and $p+l$. We then define $k=p+l$ and extend its summation range from $k=0$ to $+\infty$, introducing an exponentially small error in the mesoscopic regime $\bar{n}\gg 2J$. The resulting vector is now our mesoscopic approximation to $|\Psi_m^X(t)\rangle$. It is obtained as a tensor product

$$|\Psi_m^X(t)\rangle \simeq e^{-igmt\sqrt{\bar{n}}}|D_m(t)\rangle \otimes |\psi_m(t)\rangle, \tag{A5}$$

where $|D_m(t)\rangle$ and $|\psi_m(t)\rangle$ are defined, respectively, by Eqs. (15) and (14). Equation (16) is recovered by expanding $|J,m_0\rangle$ over the atomic polarizations at initial time $|D_m(0)\rangle$ $(-J\leq m\leq J)$.

APPENDIX B: ROTATION MATRICES

Matrix elements of SU(2) general elements are given, for example, in Ref. [32]. The matrix elements $R_{m,m'}=\langle J,m'|\exp(i\pi J^y/2)|J,m\rangle$ needed in the present paper are

$$R_{m',m} = \sqrt{\frac{(J-m)!\,(J-m')!}{(J+m)!\,(J+m')!}} \times \sum_{k=0}^{J-\max(m,m')} \frac{(-1)^{J-k}(2J-k)!}{2^{J-k}k!\,(J-m-k)!\,(J-m'-k)!}.$$

Starting from excited atoms and looking for the probability of detecting finally all the atoms in the excited state involves

$$R_{m,J} = (-1)^{J-m}R_{J,m} = \frac{1}{2^J}\sqrt{\frac{(2J)!}{(J-m)!\,(J+m)!}}.$$

APPENDIX C: DECOHERENCE AND PHASE DIFFUSION

In the $\gamma t\gtrsim 1$ case, the decay of the average photon number $\bar{n}(t)=\bar{n}\,e^{-\gamma t}$ prevents the sequence of quantum jumps from being a renewal process with a stationary waiting times probability distribution. Nevertheless, the probability that no quantum jump happens between t and $t+\tau$ knowing that one occurred at time t is given by

$$\Pi_0(t,\tau) = \prod_{t\leq t'\leq t+\tau}[1-\gamma\bar{n}(t')dt'] = \exp\left(-\gamma\int_0^\tau \bar{n}(t+\tau')d\tau'\right). \tag{C1}$$

The probability distribution for having quantum jumps at times t and $t+\tau$ is therefore given by

$$\psi(t,\tau) = -\frac{\partial \Pi_0}{\partial \tau} = \gamma \bar{n}(t+\tau) e^{-\gamma \int_0^\tau \bar{n}(t+\tau')d\tau'}. \tag{C2}$$

The probability for having exactly p quantum jumps between 0 and t at times $0 \le t_1 \le \cdots \le t_p \le t$ is equal to $\mathcal{P}_{[0,t]} \times (t_1, \ldots, t_p) = \psi(0,t_1)\psi(t_1,t_2)\cdots\psi(t_{p-1},t_p)\Pi_0(t_p, t-t_p)$:

$$\mathcal{P}_{[0,t]}(t_1, \ldots, t_p) = e^{-\gamma \int_0^t \bar{n}(t')dt'} \prod_{k=1}^{p} [\gamma \bar{n}(t_k)]. \tag{C3}$$

Using the exponential relaxation of the mean photon number $[\bar{n}(t) = \bar{n}e^{-\gamma t}]$, this leads to a Poisson distribution law for the number $N[0,t]$ of photons emitted between 0 and t with average value $\bar{n}(1-e^{-\gamma t})$. Therefore, the decoherence coefficient is equal to

$$\langle e^{i\theta N[0,t]} \rangle = \exp[\bar{n}(e^{i\theta} - 1)(1 - e^{-\gamma t})] \tag{C4}$$

which is exactly the solution of the master Eq. (26).

APPENDIX D: EFFECT OF DISSIPATION ON THE ATOMS + CAVITY

We consider the dissipative dynamics of the strongly coupled atoms + cavity systems in the mesoscopic regime. For weak dissipation $\gamma \ll g$, we show that a family of generalized Gea-Banacloche states is stable under an effective stochastic dynamics naturally arising from these approximations. We then consider the evolution of the states $|\Psi_m^X\rangle$ $(-J \le m \le J)$ and show that each of them decoheres on a time scale much longer than the decay time of the $|\Psi_{m_+}^X\rangle\langle\Psi_{m_-}^X|$ coherence for $m_+ \neq m_-$. These results validate the simplified analysis presented in Sec. III B.

1. Effective stochastic dynamics in the mesoscopic regime

The non-Hermitian Hamiltonian that describes the dynamics of the atoms + cavity system between quantum jumps is $H_{\mathrm{TC}} - i\hbar\gamma a^\dagger a/2$, where H_{TC} is the Tavis-Cummings Hamiltonian (3). Replacing H_{TC} by the effective Hamiltonian (12) leads to an effective non-Hermitian Hamiltonian over each subspace $\mathcal{H}_p$:

$$H = \hbar g\sqrt{p+c}\mathcal{J}^x - i\frac{\hbar\gamma}{2}(p + J - \mathcal{J}^z). \tag{D1}$$

The constant term $i\hbar J\gamma/2$ can be discarded in the evolution between quantum jumps since it is canceled by the normalization of the state vector. It is then useful to decompose the atoms + cavity vector over $\oplus_p \mathcal{H}_p$ as

$$|\Psi(t)\rangle = \mathcal{N}(t)\sum_{p=0}^{\infty} \frac{\alpha(t)^p}{\sqrt{p!}}|\Psi_p(t)\rangle, \tag{D2}$$

where $|\Psi_p(t)\rangle$ belongs to $\mathcal{H}_p$, $\alpha(t)$ denotes some time dependent function and $\mathcal{N}(t)$ is the normalization factor. Taking $\alpha(t) = \alpha(0)e^{-\gamma t/2}$ enables to absorb the p-dependent part in the non-Hermitian term of Eq. (D1). As a consequence, each vector $|\Psi_p(t)\rangle$ evolves in $\mathcal{H}_p$ under the non-Hermitian Hamiltonian

$$H_p = \hbar g\sqrt{p+c}\mathcal{J}^x + i(\hbar\gamma/2)\mathcal{J}^z. \tag{D3}$$

The time dependence of α reflects the acquisition of information arising from the absence of quantum jumps on the cavity. Because of the strong coupling between the atoms and the cavity, the state of the atoms is also altered and this is why dissipation has to be taken into account in the evolution of each $|\Psi_p(t)\rangle$ through the non-Hermitian term in Eq. (D3). Note that this induces a change in the probabilities for the cavity to release a photon into its environment and thus modifies the cavity relaxation.

It is possible to solve analytically the resulting Schrödinger equation for each $|\Psi_p(t)\rangle$ but the resulting expressions are very complicated. In particular, taking into account the back action of cavity dissipation through the atoms on the statistics of photon emission leads to very cumbersome expressions. Nevertheless, in the strong coupling regime of cQED $(\gamma \ll g)$, neglecting the effect of cavity dissipation on the atoms seems to be reasonable and turns out to make the problem much more tractable. For values of t such that $\bar{n}(t) = \bar{n}e^{-\gamma t} \gg 1$, we expect H_p to be dominated by its Hermitian part. Discarding the non-Hermitian part in Eq. (D3) means that each $|\Psi_p(t)\rangle$ has the same unitary evolution than in the dissipationless case. Therefore, within this approximation, the atoms + cavity state evolves in the absence of quantum jumps between 0 and t as

$$|\Psi(t)\rangle_{\mathrm{n.j.}} = e^{-\bar{n}(t)/2}\sum_{p=0}^{\infty} \frac{\alpha(t)^p}{\sqrt{p!}} e^{-igt\sqrt{p+c}\mathcal{J}^x}|\Psi_p(0)\rangle, \tag{D4}$$

where $\bar{n}(t) = |\alpha(t)|^2 = |\alpha|^2 e^{-\gamma t}$.

Let us now consider a state of the form (A3) and compute its evolution during a time t in the absence of quantum jump. Equation (D4) leads to

$$|\Psi_m^X(t)\rangle_{\mathrm{n.j.}} = e^{-\bar{n}(t)/2}\sum_{p=0}^{\infty} \frac{\alpha(t)^p}{\sqrt{p!}} e^{-igmt\sqrt{p+c}}|X_m^{(p)}\rangle. \tag{D5}$$

Note that, within the mesoscopic approximation, this state can be approximated by a factorized state of the form (A5) taking into account dissipation through the exponential decay of $\bar{n}(t)$. For $\gamma t \ll 1$, Eq. (A5) provides a good approximation to Eq. (D5).

We now consider the effect of quantum jumps on state (D5). Within the mesoscopic approximation, the action of the creation operator on states $|X_m^{(p)}\rangle$ can be simplified:

$$a|X_m^{(p)}\rangle = \sqrt{p+J-m}|J,m\rangle \otimes |p+J-m-1\rangle \simeq \sqrt{p}|X_m^{(p-1)}\rangle. \tag{D6}$$

Using this expression, we see that $a|\Psi_m^X(t)\rangle_{\mathrm{nj}}$ has the same form as (D5), the phase $e^{-igmt\sqrt{p+c}}$ in front of $|X_m^{(p)}\rangle$ being replaced by $e^{-igmt\sqrt{p+1+c}}$. This shows that all states of the form

$$|\Psi_m[\alpha, \{\Phi(t)\}]\rangle = e^{-\bar{n}(t)/2}\sum_{p=0}^{\infty} \frac{\alpha(t)^p}{\sqrt{p!}} e^{-i\phi(p,t)}|X_m^{(p)}\rangle, \tag{D7}$$

where $\Phi(t)$ denotes the set of all phases $\phi(p,t)$ $(p \ge 0)$ at time t, form a stable class along the stochastic evolution. The phases $\phi(p,t)$ follow a stochastic trajectory consisting of

smooth deterministic evolution periods between quantum jumps. The deterministic evolution is ruled by $\dot{\phi}(p,t)=mg\sqrt{p+c}$. The quantum jumps correspond to discontinuous steps $\phi(p,t^+)=\phi(p+1,t)$.

2. Solution for the states $|\Psi_m^X\rangle$

Studying the evolution of a superposition of states of the form (A3) leads to consider the evolution of a coherence between $|\Psi_{m_+}^X\rangle$ and $|\Psi_{m_-}^X\rangle$. After time t, the stochastic evolution of $|\Psi_{m_+}^X\rangle\langle\Psi_{m_-}^X|$ produces an ensemble of projectors of the form $|\Psi_{m_+}[\alpha,\{\Phi_+(t)\}]\rangle\langle\Psi_{m_-}[\alpha,\{\Phi_-(t)\}]|$. Denoting by $\rho_{m_+,m_-}(t)$ the operator obtained by averaging these projectors over the measure given by the stochastic trajectories, we obtain

$$\rho_{m_+,m_-}(t)=e^{-\bar{n}(t)}\sum_{(p_-,p_+)}\frac{\alpha(t)^{p_-+p_+}}{\sqrt{p_-!\,p_+!}}D_{p_-,p_+}(t)|X_{m_+}^{(p_+)}\rangle\langle X_{m_-}^{(p_-)}|, \tag{D8}$$

where $D_{p_+,p_-}(t)$ denotes the average over all stochastic trajectories of the relative phase factor $e^{i[\phi_+(p_-,t)-\phi_-(p_+,t)]}$, where the phases $\phi_\pm(p,t)$ are relative to the states $\Psi_{m_\pm}$. Because the quantum jump process is memoryless, these averages obey the following set of coupled first order differential equations

$$\dot{D}_{p_+,p_-}(t)=\gamma\bar{n}(t)[D_{p_++1,p_-+1}(t)-D_{p_+,p_-}(t)]-i\Omega_{p_-,p_+}^{(m_-,m_+)}D_{p_+,p_-}(t), \tag{D9}$$

where

$$\Omega_{p_+,p_-}^{(m_-,m_+)}=g(m_+\sqrt{p_++c}-m_-\sqrt{p_-+c}). \tag{D10}$$

Let us first focus on the case $m_+=m_-=m$. Probing the (p_+,p_-) dependence of $D_{p_+,p_-}(t)$ gives us an insight of the decoherence of the initial pure state $|\Psi_m^X\rangle$ of the atoms + cavity system. Decoherence arises from the quantum jumps that lead to the spreading of $\phi(p_+,t)-\phi(p_-,t)$. Let us estimate the decoherence coefficient between $|X_m^{(p_+)}\rangle$ and $|X_m^{(p_-)}\rangle$ within the mesoscopic approximation. Expanding $\sqrt{p+c+1}\simeq\sqrt{p+c}+1/2\sqrt{p}$ the phase factor associated with a single jump at time t_j is $gmt_j/2\sqrt{p_+}-gmt_j/2\sqrt{p_-}$ which is approximately equal to $gmt_j(p_--p_+)/4\bar{n}^{3/2}$ for $p_\pm$ close to $\bar{n}$ (we assume $\gamma t_j\lesssim 1$ for simplicity). Thus, for $m_+=m_-=m$, the decoherence factor $D_{p_+,p_-}(t)$ can be approximated by

$$D_{p_+,p_-}(t)\simeq e^{-igmt(\sqrt{p_++c}-\sqrt{p_-+c})}\langle e^{i[(p_+-p_-)/2\bar{n}]\Sigma_j gmt_j/2\sqrt{\bar{n}}}\rangle. \tag{D11}$$

Remembering that the statistics of occurrence times of quantum jumps for all states of the form (D7) is computed in Appendix C, we immediately obtain ($\gamma t\lesssim 1$)

$$D_{p_+,p_-}(t)\simeq e^{-igmt(\sqrt{p_++c}-\sqrt{p_-+c})}\,e^{\bar{n}\gamma\int_0^t(e^{i\eta_{p_+,p_-}\theta_m(\tau)}-1)d\tau}, \tag{D12}$$

where $\theta_m(\tau)=gm\tau/2\sqrt{\bar{n}}$ and $\eta=(p_+-p_-)/2\bar{n}$. The second factor in Eq. (D12) is responsible for decoherence of the state $|\Psi_m^X\rangle$ of the atoms + cavity system. Because of the amplitude $e^{-\bar{n}(t)/2}\frac{\alpha(t)^{p_\pm}}{\sqrt{p_\pm!}}$ in the atoms + cavity states, the values of $p_\pm$ that contribute to the sum lie within $|p_+-p_-|\lesssim\sqrt{\bar{n}(t)}$ and therefore $|\eta|\ll 1$ within the mesoscopic regime and for $\gamma t\lesssim 1$. That's why decoherence of a state (A3) can be neglected as in Ref. [11].

Before moving on the $m_+\neq m_-$ case, it is interesting to see how his results (Sec. III A) are recovered within the present approach. Following Ref. [11], we ignore the discrete character of p and replace the finite difference equation (D9) by partial differential equation. Solving this equation can easily be done using the characteristics method. Starting from the initial condition $|\Psi_m^X\rangle$, this leads to $\rho_{m,m}(t)=|\Psi_m(t)\rangle\langle\Psi_m(t)|$, where

$$|\Psi_m(t)\rangle=e^{-\bar{n}(t)/2}\sum_{p=0}^{\infty}\frac{\alpha(t)^p}{\sqrt{p!}}e^{-i\Theta(p,t)}|X_m^{(p)}\rangle \tag{D13}$$

and

$$\Theta(p,t)=gm\int_0^t\sqrt{c+p+\bar{n}(\tau)-\bar{n}(t)}d\tau. \tag{D14}$$

Evaluating the integral and for all p leads to expressions corresponding to Eqs. (18a)–(18c) of Ref. [11].

The case $m_+\neq m_-$ can then be studied along the same lines. Within the mesoscopic approximation, the phase jump associated with a quantum jump occurring at time t_j can be evaluated as $\exp[igt_j(m_--m_+)/2\sqrt{\bar{n}(t_j)}]$. Note that it does not vanish for $p_+=p_-\simeq\bar{n}(t_j)$. This is why decoherence for $m_+\neq m_-$ occurs on a much shorter time scale than the decoherence of the state $|\Psi_m^X\rangle$. In principle, $\rho_{m_+,m_-}(t)$ could be computed from the formalism presented here but this is not necessary for the present purpose. In the $\gamma t\ll 1$ case, the problem can be simplified by considering that the evolution of the atoms + cavity state with initial condition $|\Psi_m^X\rangle$ produces a pure state as in the previous paragraph and by approximating this pure state by $|\Psi_m^X(t)\rangle$ [see Eq. (35)]. The argumentation presented in Sec. III B then leads to the decoherence properties of the atoms + cavity state suitable for this regime.

[1] J.-M. Raimond, M. Brune, and S. Haroche, Rev. Mod. Phys. **73**, 565 (2001).
[2] M. Brune, E. Hagley, J. Dreyer, X. Maître, A. Maali, C. Wunderlich, J.-M. Raimond, and S. Haroche, Phys. Rev. Lett. **77**, 4887 (1996).
[3] A. Auffeves, P. Maioli, T. Meunier, S. Gleyzes, G. Nogues, M. Brune, J.-M. Raimond, and S. Haroche, Phys. Rev. Lett. **91**, 230405 (2003).
[4] T. Meunier, S. Gleyzes, P. Maioli, A. Auffeves, G. Nogues, M. Brune, J.-M. Raimond, and S. Haroche, Phys. Rev. Lett. **94**, 010401 (2005).
[5] G. Morigi, E. Solano, B.-G. Englert, and H. Walther, Phys. Rev. A **65**, 040102(R) (2002).
[6] P. Maioli, T. Meunier, S. Gleyzes, A. Auffeves, G. Nogues, M. Brune, J. M. Raimond, and S. Haroche, Phys. Rev. Lett. **94**, 113601 (2005).
[7] J. Gea-Banacloche, Phys. Rev. A **44**, 5913 (1991).
[8] P. Knight and B. Shore, Phys. Rev. A **48**, 642 (1993).
[9] A. B. Klimov and S.M. Chumakov, Phys. Lett. B **202**, 145 (1995).
[10] J. Dalibard, Y. Castin, and K. Molmer, Phys. Rev. Lett. **68**, 580 (1992).
[11] J. Gea-Banacloche, Phys. Rev. A **47**, 2221 (1993).
[12] A. Blais, R.-S. Huang, A. Wallraff, S. M. Girvin, and R. J. Schoelkopf, Phys. Rev. A **69**, 062320 (2004).
[13] M. Tavis and F. Cummings, Phys. Rev. **170**, 379 (1968).
[14] E. Jaynes and F. Cummings, Proc. IEEE **51**, 89 (1963).
[15] V. Buzek, H. Moya-Cessa, P.L. Knight, and S. J. D. Phoenix, Phys. Rev. A **45**, 8190 (1992).
[16] P. Bertet, S. Osnaghi, A. Rauschenbeutel, G. Nogues, A. Auffeves, M. Brune, J.-M. Raimond, and S. Haroche, Nature (London) **411**, 166 (2001).
[17] J. C. Retamal, C. Saavedra, A. B. Klimov, and S. M. Chumakov, Phys. Rev. A **55**, 2413 (1997).
[18] P. Milman, Y. Castin, and L. Davidovich, Phys. Rev. A **61**, 063803 (2000).
[19] J. Schriefl, M. Clusel, D. Carpentier, and P. Degiovanni, Phys. Rev. B **72**, 035328 (2005).
[20] C. Saavedra, A. B. Klimov, S. M. Chumakov, and J. C. Retamal, Phys. Rev. A **58**, 4078 (1998).
[21] R. Feynman and F. Vernon, Ann. Phys. (N.Y.) **24**, 118 (1963).
[22] M.S. Kim and V. Buzek, Phys. Rev. A **46**, 4239 (1992).
[23] M. Brune, F. Schmidt-Kaler, A. Maali, J. Dreyer, E. Hagley, J.-M. Raimond, and S. Haroche, Phys. Rev. Lett. **76**, 1800 (1996).
[24] P. Bertet, A. Auffeves, P. Maioli, S. Osnaghi, T. Meunier, M. Brune, J.-M. Raimond, and S. Haroche, Phys. Rev. Lett. **89**, 200402 (2002).
[25] A. Wallraff, D. I. Schuster, A. Blais, L. Frunzio, R.-S. Huang, J. Majer, S. Kumar, S. M. Girvin, and R. J. Schoelkopf, Nature (London) **431**, 162 (2004).
[26] A. Wallraff, D. I. Schuster, A. Blais, L. Frunzio, J. Majer, M. H. Devoret, S. M. Girvin, and R. J. Schoelkopf, Phys. Rev. Lett. **95**, 060501 (2005).
[27] L. Frunzio, A. Wallraff, D. I. Schuster, J. Majer, and R. J. Schoelkopf, IEEE Trans. Appl. Supercond. **15**, 860 (2005).
[28] A. Lupascu, E. Driessen, L. Roschier, C. Harmans, and J. Mooij, cond-mat/0601634 (unpublished).
[29] I. Siddiqi, R. Vijay, F. Pierre, C. M. Wilson, L. Frunzio, M. Metcalfe, C. Rigetti, R. J. Schoelkopf, M. H. Devoret, D. Vion, and D. Esteve, Phys. Rev. Lett. **94**, 027005 (2005).
[30] I. Siddiqi, R. Vijay, F. Pierre, C. Wilson, L. Frunzio, M. Metcalfe, C. Rigetti, and M. H. Devoret, cond-mat/0507248 (unpublished).
[31] Y. Makhlin, G. Schoen, and A. Shnirman, Chem. Phys. **296**, 315 (2004).
[32] F. Arrecchi, E. Courtens, R. Gilmore, and H. Thomas, Phys. Rev. A **6**, 2211 (1972).